Israel Journal of Chemistry

IJC

Official Journal of the Israel Chemical Society

REPRINT

www.ijc.wiley-vch.de

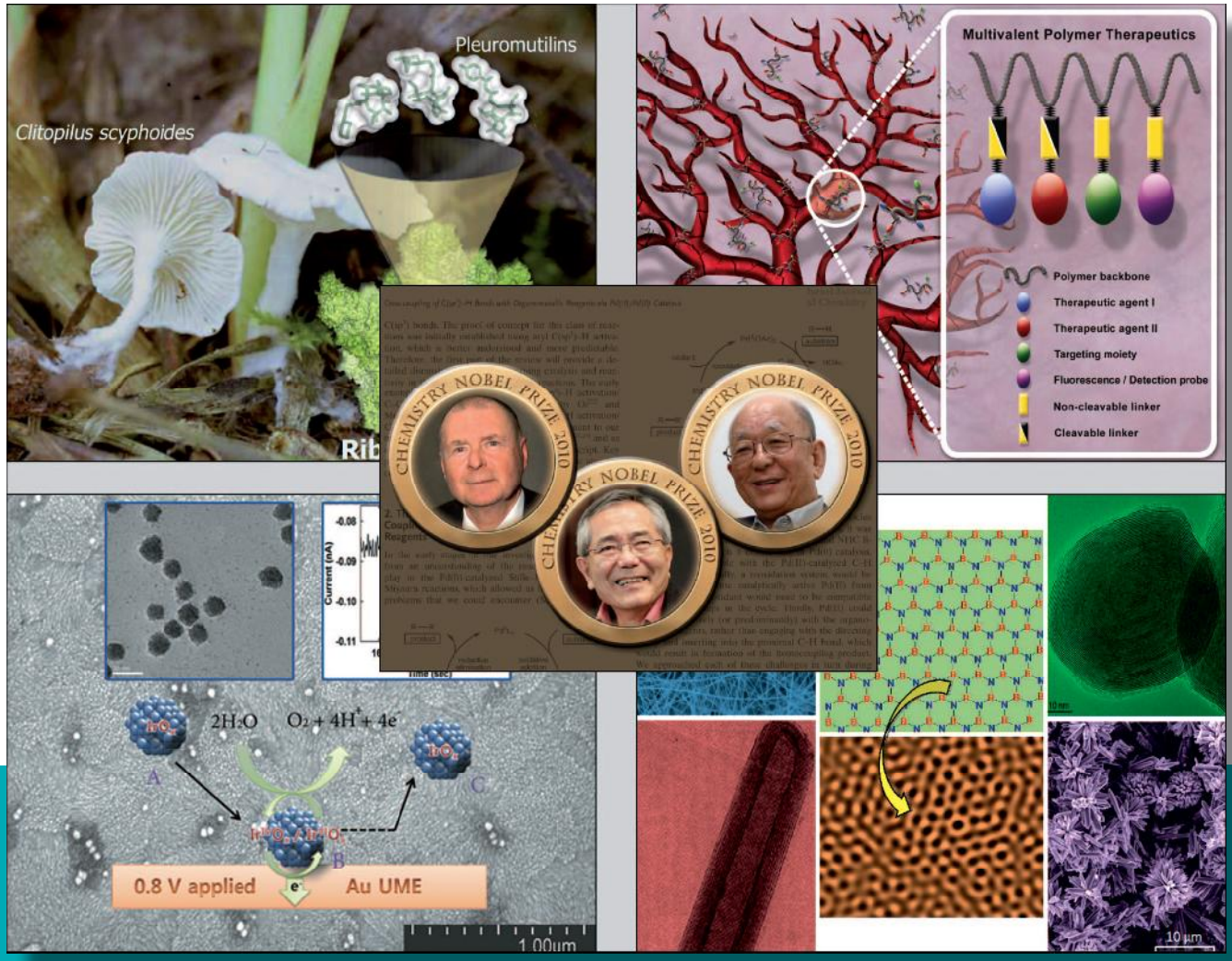

WILEY-VCH

Israel Journal of Chemistry

Official Journal of the Israel Chemical Society

Table of Contents

WILEY-VCH

DOI: 10.1002/ijch.201100161

Molecular Alignment Induced by Ultrashort Laser Pulses and Its Impact on Molecular Motion

Sharly Fleischer,[a, b] Yuri Khodorkovsky,*[a] Erez Gershnabel,[a] Yehiam Prior,[a] and Ilya Sh. Averbukh[a]

Abstract: Spectroscopy aims at extracting information about matter through its interaction with light. However, when performed on gas and liquid phases as well as solid phases lacking long-range order, the extracted spectroscopic features are in fact averaged over the molecular isotropic angular distributions. The reason is that light–matter processes depend on the angle between the transitional molecular dipole and the polarization of the light interacting with it. This understanding gave birth to the constantly expanding field of "laser-induced molecular alignment". In this paper, we attempt to guide the readers through our involvement (both experimental and theoretical) in this field in the last few years. We start with the basic phenomenon of molecular alignment induced by a single pulse, continue with selective alignment of close molecular species and unidirectional molecular rotation induced by two time-delayed pulses, and lead up to novel schemes for manipulating the spatial distributions of molecular samples through rotationally controlled scattering off inhomogeneous fields and surfaces.

Keywords: molecular alignment · femtosecond laser pulses · control of molecular rotation and motion · rotational spectroscopy

1. Introduction

In recent years, the interest in molecular alignment and orientation has been constantly increasing, and a large variety of applications in chemistry, physics, nanoscience, and nonlinear optics has been demonstrated. The topic of molecular alignment has been reviewed,[1,2] and therefore the main emphasis in this article is on manipulation and control of molecular rotations by ultrashort laser pulses. Femtosecond pulses are commonly used for exciting and probing the internal molecular degrees of freedom, and thus provide good means for controlling the slowest of them all, namely, molecular rotations. The control schemes presented hereafter utilize non-resonant interactions and therefore are not molecule-specific.

We first discuss the basic principles of laser-induced molecular alignment, both classically and quantum mechanically. Next, we explore control schemes based on the interaction of the molecules with two properly delayed laser pulses, for selective rotational excitation of molecular species with close chemical and physical properties such as molecular isotopes (isotopologues),[3] and molecular nuclear spin isomers[4,5] (para and ortho). The first pulse interacts with an isotropic thermal molecular ensemble; it excites rotational states leading to dynamic molecular evolution under field-free conditions after the pulse is over. The effect of a delayed second pulse depends on the molecular angular distribution and momentum at the time of interaction. Changing the relative polarization of the pulses will be shown to effectively control the sense of rotation (clockwise/counterclockwise). Such manipulations create a highly anisotropic angular distribution, and offer an efficient way for controlling the chemical kinetics as well as the optical properties of the medium.[6,7] In the second part of this review, we discuss two novel schemes for controlling the spatial distribution of molecular samples via the scattering of rotationally excited molecules off inhomogeneous fields[8,9] and off surfaces.[10]

In the quest for better control of molecular angular distribution, a number of methods have been used to orient molecules via interaction with static or time-dependent electromagnetic fields.[1] Renewed interest in these problems was triggered by experiments demonstrating that intense, ultrashort laser pulses tend to align the molecular axis along the direction of the field polarization (for early experiments see refs. [11–14]). When a laser pulse acts on a molecule, it induces an electric dipole in the molecule, which in turn interacts with the laser electric field. Since molecular polarizability is generally anisotropic, such an interaction leads to the alignment of the molecule along

[a] S. Fleischer, Y. Khodorkovsky, E. Gershnabel, Y. Prior, I. S. Averbukh
Department of Chemical Physics
Weizmann Institute of Science
Rehovot 76100, Israel

[b] S. Fleischer
Present address: Department of Chemistry
Massachusetts Institute of Technology
Cambridge, MA 02139, USA

the direction of the laser pulse polarization. A strong enough CW laser field creates pendular molecular states[15–17] that are hybrids of field-free rotor eigenstates. By adiabatically turning the laser field on, it is possible to trap a molecule in the ground pendular state, thus leading to molecular alignment. Early studies on laser-induced molecular alignment used pulses of nanosecond durations, much longer than the molecular rotational time scale (typically a few picoseconds). Under these conditions, significant molecular alignment takes place, but only under the constant action of the intense aligning field. Already then it was well understood that non-adiabatic excitation by short laser pulses induces long-persisting beats of the molecular alignment signal in the molecular angular distribution.[18–22]

For quite some time it had been realized that ultrashort (on the order of 100 fs) pulse excitation of molecular rotational wave packets may result in considerable transient molecular alignment after the laser pulse is over, that is, under field-free conditions.[23–30] A linear molecule subject to an electric field tends to align parallel to the applied field direction. Once created, an aligned

Sharly Fleischer received his B.Sc. in Chemistry from Ben-Gurion University of the Negev, Israel. He did his Ph.D. in the Chemical Physics department at the Weizmann Institute of Science with Prof. Yehiam Prior and in close collaboration with Prof. Ilya Sh. Averbukh in the field of laser-induced molecular alignment. Since 2010 he has been working on coherent control and spectroscopy with THz fields as a postdoctoral associate in Prof. Keith A. Nelson's lab at Massachusetts Institute of Technology (MIT).

Yuri Khodorkovsky received his B.Sc. and M.Sc. degrees in Chemistry at the Ben-Gurion University of the Negev, in Beer-Sheva, Israel. Currently, he is working on his Ph.D. thesis as part of the theoretical group of Prof. Ilya Sh. Averbukh, at the Weizmann Institute of Science, in Rehovot, Israel. His main topic of research is controlling molecular rotation by one or several ultrashort laser pulses, and its applications to molecule-surface scattering and molecular collision processes.

Erez Gershnabel received his B.Sc. degrees in Physics and Electrical Engineering in 2001 from the Tel-Aviv University, Tel-Aviv, Israel. In 2003, he obtained his M.Sc. degree in Physics, from the Weizmann Institute of Science, Rehovot, Israel. In 2011, he obtained his Ph.D. degree from the Weizmann Institute of Science, where he studied laser-induced molecular alignment and orientation.

Yehiam Prior received his B.Sc. at the Hebrew University of Jerusalem, and his Ph.D. in Physics from the University of California at Berkeley (1977). Following his postdoctoral work at Harvard he joined the Department of Chemical Physics at the Weizmann Institute of Science in Israel. Since then, he has chaired this department, headed the Institute's Division of Information Systems, chaired the Institute's Scientific Council of tenured professors, and since 2006, he is the Dean of the Faculty of Chemistry. His research focuses on light matter interaction, nonlinear and ultrafast optics, and laser material processing, with recent work on near field microscopy and nanophotonics.

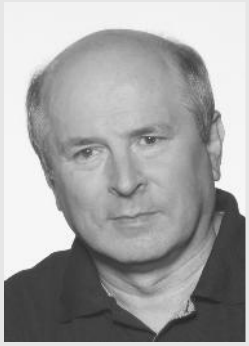

Ilya Averbukh graduated from the Kolmogorov Boarding School for Physics and Mathematics (Moscow State University) in 1969, and received his M.Sc. in Physics and M.Sc. in Applied Mathematics from Novosibirsk State University (1974). He then joined the Institute for Applied Physics (Academy of Sciences, Moldova) as a Researcher, received his Ph.D. from IAP in 1981, and finally became a Lead Scientist of the Institute. Since 1991 he has been with the Weizmann Institute of Science (Israel), where he currently holds the Bildner Professorial Chair in the Department of Chemical Physics. Ilya Averbukh is a Fellow of APS and OSA. His research focuses on various theoretical aspects of light-matter interactions, ranging from quantum optics to coherent and nonlinear optics and ultrafast spectroscopy.

state will periodically regenerate due to the effect of quantum revivals.[23,27,31–33] This phenomenon paves the way for many applications that require transient molecular alignment when the molecular angular distribution briefly becomes narrow at some predetermined time. A number of such applications are discussed in ref. [34], including the use of field-free aligned molecules for quantum information processing (for the first experimental demonstration see refs. [35–37]), pulse compression,[38] and phase modulation by rotational wavepacket revivals.[39,40]

In the last few years, pre-alignment of molecules has been used extensively for generation of high harmonics,[41,42] control of photoelectron angular distribution due to strong field ionization,[43] and for molecular fragmentation imaging.[44] Molecular alignment has been shown to play a significant role in filamentation of strong ultrashort laser pulses.[45–47] New X-ray laser sources such as the free electron X-ray laser at SLAC (Stanford Linear Accelerator Center) National Accelerator Laboratory are predicted to yield X-ray diffraction images from femtosecond X-ray laser pulses, a process that requires a high degree of molecular alignment at the moment of interaction.[48,49] And the list of applications is constantly growing.

The quality of the alignment of a linear molecule is usually described by the maximal value of the alignment factor $\langle \cos^2\theta \rangle$ that is obtained by an ensemble of laser-excited molecules. Here θ is the angle between the molecular axis and the polarization of the laser electric field, and the angular brackets denote averaging over the molecular ensemble. It was shown that the maximal degree of molecular alignment attainable by a single, ultrashort laser pulse is limited,[50] and even before this theoretical limit is reached, practical limits are imposed on the strength of the aligning field by such processes as field-induced ionization and dissociation. A solution to the problem of a too strong input pulse was suggested by dividing the input energy between multiple properly delayed laser pulses,[28,50–53] and later demonstrated[54–56] to yield a high degree of transient molecular alignment.

Several techniques have been applied for the detection of molecular alignment. The alignment-induced birefringence may be detected by a weak probe pulse propagating through the sample.[57] Aligned molecules may be Coulomb exploded and the fragments detected and their energy and momentum analyzed to determine the angular distribution of the molecules prior to the dissociation.[58–60] In our experimental work, we mostly used degenerate four-wave mixing (DFWM) in a forward-propagating configuration,[61] a method used extensively by the Dantus group[62,63] to study various aspects of laser-induced alignment. To complete this list of experiments one should mention that more complex molecules such as iodobenzene and methyl iodide may be laser aligned,[64] alignment-dependent photo-dissociation of linear molecules such as N_2,[65] I_2,[66] and CO[67] was demonstrated, and a higher degree of alignment was achieved by means of pulse shaping as well.[68,69]

2. Creating and Detecting Field-Free Alignment

2.1. Theoretical background

When a polar linear molecule (such as HCl, KI, etc.) interacts with a DC electric field, a torque, proportional to $\tau \propto -\sin(\theta)$, is exerted on the molecule, and orients it parallel to the field polarization (here θ is the angle between the molecular axis and the electric field polarization). When the same linear molecule interacts with an intense fast oscillating AC electric field (i.e., a femtosecond laser pulse), the laser field induces an electric dipole and interacts with it. The interaction energy is given by:

$$V = -\frac{1}{4}E^2\left(\Delta\alpha\cos^2\theta + \alpha_\perp\right) \tag{1}$$

where E is the envelope of the laser electric field, and $\Delta\alpha = \alpha_\parallel - \alpha_\perp$ and $\alpha_\parallel, \alpha_\perp$ are the parallel and perpendicular polarizability components of the molecule, respectively. Thus, the torque exerted on the molecule is given by $\tau \propto dV/d\theta \propto -\sin(2\theta)$. For the sake of simplicity, let us first consider the effect of such interaction on a two-dimensional ensemble of molecules distributed isotropically in a plane at zero temperature. The torque exerted on a molecule initially aligned at an angle θ to the field polarization is proportional to $-\sin(2\theta)$. A typical rotational time for a small molecule is on the order of a picosecond. Thus, during the femtosecond pulse duration the molecule may be regarded as "frozen" while its angular momentum is dramatically changed by the torque applied by the laser. Since the laser pulse is short compared to the rotational dynamics of the molecule, it may be approximated as a delta-function, and the angular velocity that a molecule gains is proportional to the torque exerted by the field, as depicted in Figure 1a. Propagation of the molecules with their acquired angular velocities results in

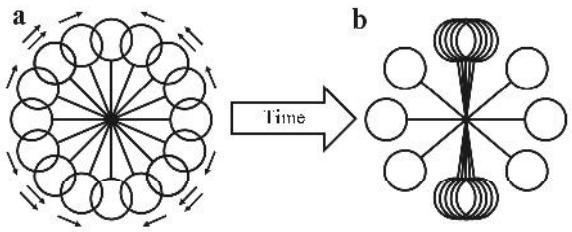

Figure 1. (a) Schematic representation of isotropically distributed molecules subject to an ultrashort laser pulse polarized along the vertical direction, inducing angular velocities as depicted by the black arrows. (b) Field-free rotation of the molecules according to their acquired angular velocities results in a transient, highly anisotropic, angular distribution ("alignment") following the interaction with the ultrashort pulse.

a squeezed angular distribution, which peaks along the applied field polarization axis (Figure 1 b).

The typical time for a small molecule to align is a few hundreds of femtoseconds (depending on the pulse intensity and on the molecular mechanical and electrical properties). Classically, in the absence of additional fields, the molecules will continue to rotate past their alignment event shown in Figure 1 b, and will never reach the same degree of alignment again. However, due to the discreteness of the rotational energy levels and their associated commensurate energies, rotational quantum revivals,[70,71] manifested as periodically occurring squeezed angular distributions following the initial pulse, are observed.

Quantum-mechanically, a rotational wave packet can be written as a superposition of the eigenstates of a rigid rotor:

$$|\psi(\theta,t)\rangle = \sum_{J,m} c_{Jm}|J,m\rangle \exp(-iE_J t/\hbar) \tag{2}$$

where $|J,m\rangle$ are the rigid rotor eigenvectors (corresponding to the Y_J^m spherical harmonic eigenfunctions) and c_{Jm} are the expansion coefficients. For linear molecules, the energy spectrum is given by $E_J = hBc\,J(J+1)$ (where $B = \hbar/(4\pi Ic)$ is the rotational constant, c is the speed of light, and I is the molecular moment of inertia). Due to the quantization of the rotational energies, the rotational wavepacket periodically reproduces itself when all of the oscillating terms in Equation 2 accumulate a phase which is an integer multiple of 2π, that is, at integer multiples of $T_{rev} = 1/(2Bc)$, termed as "rotational revival time". Thus the wavefunction is periodic, $\psi(t) = \psi(t + T_{rev})$, as are all the corresponding observables (here we mostly focus on the alignment factor $\langle\cos^2\theta\rangle$; however, this claim is general and apply for all other observables as well).

In what follows, we use the classical description and quantum mechanical periodic character of the system in order to predict the angular distribution of the molecular ensemble as a function of time. In the classical picture (Figure 1) we have seen that following the interaction with a short laser pulse the (initially isotropic) molecular ensemble attains a transiently squeezed angular distribution which is referred to as "alignment" or "cigar-like" distribution. It has been previously shown that the classical and the quantum mechanical approaches agree at short times after the pulse, around $t = 0$,[7,50] thus the classically derived aligned distribution reappears after each and every integer multiple of the quantum revival time T_{rev}. Furthermore, the aligned angular distribution is preceded by an anti-aligned angular distribution, in which the molecules are confined to the plane perpendicular to the laser field polarization axis as observed in the left panel of Figure 2. Based on the classical model in Figure 2, if it was possible to reverse the direction of time and let the rotationally excited molecules propagate backwards, instead of reaching an aligned distribution, the transient molecular angular distribution would have peaked in the perpendicular plane.

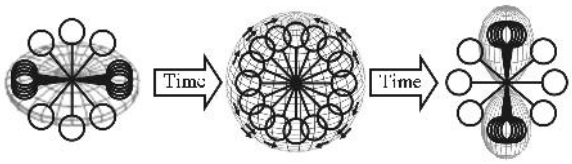

Figure 2. Evolution of the molecular ensemble shown in Figure 1 backwards in time, results in an anti-aligned molecular distribution (left panel). In the background, the corresponding 3D angular distributions are depicted.

This situation is referred to as the anti-aligned or "disk" state. Physically, time reversal is not applicable; however, since the molecular angular distribution is periodic, the "negative time" prediction is observed shortly before integer multiples of the revival time.

Moreover, the molecular angular distribution demonstrates substantial deviations from the isotropic distribution at additional moments throughout its evolution in time, such as half and quarter (three quarters) of the revival time, as will be described hereafter. At these moments of time, a more involved quantum analysis is required.

At the time of $^1/_2 T_{rev}$, the angular distribution evolves from alignment to anti-alignment through the isotropic distribution, namely, in reverse order compared to the evolution around T_{rev}. This can be derived in the following way. Consider the time dependence of the observable of interest, $\langle\cos^2\theta\rangle$ based on the rotational wavepacket evolution in time (Equation 2)

$$|\psi(\theta,\tau)> = \sum_{J,m} c_{Jm}|J,m> \exp(-i\pi J(J+1)\tau), \tag{3}$$

where we have written the time-dependent phase term explicitly, and the time τ is given in units of T_{rev}. A detailed calculation of the coefficients $c_{J,m}$ can be found in ref.[72] The alignment factor is given by:

$$\langle\cos^2\theta\rangle(\tau) = \langle\psi(\theta,\tau)|\cos^2\theta|\psi(\theta,\tau)\rangle = \\ = \sum_{J',m'}\sum_{J,m} c^*_{J'm'}c_{Jm}\underbrace{\langle J',m'|\cos^2\theta|J,m\rangle}_{\propto\delta\left\{\begin{matrix}J,J'\\J,J'\pm 2\end{matrix}\right\}\delta_{m,m'}}\underbrace{\exp(-i\pi[J'(J'+1)-J(J+1)]\tau)}_{\zeta_{JJ'}} \tag{4}$$

The observable of interest,$\cos^2\theta$, couples only eigenstates with the same m quantum number, and J numbers of the same parity. The matrix elements $\langle J',m|\cos^2\theta|J,m\rangle$ may be derived by means of the spherical harmonics recur-

rence relations.[73] For terms with the same angular momentum quantum number ($J = J'$), the time-dependent phase disappears, and this results in a time-independent contribution to the alignment factor: 1/3 for thermal isotropic distribution, and $>1/3$ for an excited, non-thermal distribution. Theoretically, for an infinitely strong pulse populating J states high above the thermal distribution and preserving the m quantum numbers of the initial thermal distribution, the time-independent (permanent) alignment may reach the value of $\langle \cos^2\theta \rangle = 1/2$. This property of rotationally excited molecules[7,56,74] will be further discussed in the beginning of Section 4.

For the terms with $J = J' \pm 2$, the time dependence is given by the phase factors:

$$\zeta_{J,J\pm2}(\tau) = \exp(-i\pi\tau(4J+6)) \tag{5}$$

In what follows, we briefly describe the transient alignment factor at several key points in time, based on our previous classical description and on the state-specific time-dependent phase in Equation 5. We have seen that, following a short laser pulse, the molecules transiently align along the field polarization axis. At integer revival times ($\tau = 0, 1, 2, ...$), the phase term $\zeta_{J,J\pm2}$ is equal to unity for all J quantum numbers.

By setting $\tau = 1/2$ in Equation 5, one immediately sees that the phase terms are π-shifted for all of the J's, resulting in $\zeta_{J,J\pm2} = -1$. Therefore, all of the phase factors (for different J's) are "in phase" and thus contribute constructively to the overall angular distribution, however with a negative sign, peaking in the negative direction but with the same magnitude (Figure 3c at $\tau = 1/2$). This reversed angular distribution evolution plays a key role in controlling and selective addressing of molecular isotopes in a mixture.

At quarter revival time ($\tau = 1/4, 1\,1/4, ...$) the situation is slightly more complex, since the phase term $\zeta_{J,J\pm2}$ assumes different phases depending on the J-state parity (even or odd). For even J states at $\tau = 1/4$, $\zeta_{J,J\pm2} = i$ while for odd J states $\zeta_{J,J\pm2} = -i$. Thus the even states contribute to the signal "in phase" among themselves, and so do the odd states. However, the two parity manifolds interfere destructively, since their contributions are π-shifted with respect to one another. In addition, the time-dependent signal is different (shifted by $\pi/2$) with respect to what is observed at integer and at half revivals (Figure 3a, 3b). At three-quarters revival, the phases are shifted by $\pi/2$ with respect to the quarter revival. The opposing time-dependent alignment factors of the even and odd manifolds around the $1/4$ ($3/4$) revival times play a significant role in selective excitation of nuclear spin modifications, as will be discussed shortly.

Figure 3 summarizes the alignment factor evolution following the rotational excitation of diatomic molecules, calculated separately for even (3a) and odd (3b) rotational states and for a thermal ensemble (3c) of homonuclear diatomics with atomic nuclear spins $I = 1/2$ (for which the odd/even population ratio is 3/1[75]).

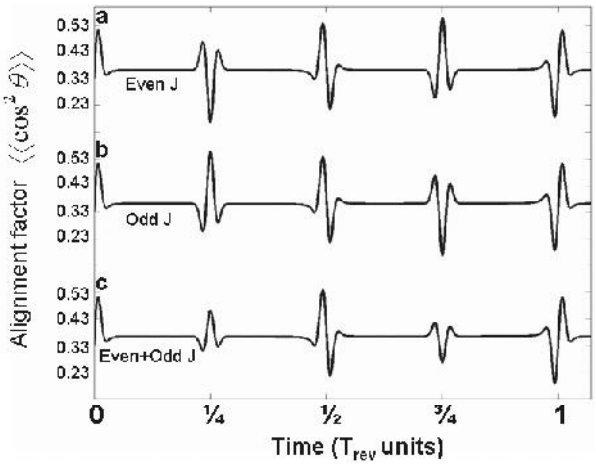

Figure 3. Time dependence of the alignment factor of $^{15}N_2$ molecules at room temperature for: (a) even rotational states only, (b) odd rotational states only, and (c) 3:1 mixture of odd:even rotational states (natural case).

Due to the nuclear spin statistical ratio of 3/1 for odd/even state populations, the two opposing quarter-revival signals do not cancel each other, and the averaged angular distribution becomes anisotropic, however, with reduced amplitude compared to the full and half revival times. Note that for heteronuclear diatomics, where the nuclear spin statistics does not play a role, the even and odd rotational states are equally populated in a thermal ensemble and the contributions of the even and odd states completely cancel each other.

2.2. Experimental Techniques: Creating and Detecting Field-Free Alignment

As discussed, the laser-induced alignment modifies the optical properties of the molecular sample. The experimental techniques used hereafter make use of these changes (i.e., birefringence). Thus, for example, a field polarized parallel to the axis of alignment will experience an increased refractive index $n_{cigar} > \bar{n}$, while for an anti-aligned (disk) $n_{disk} < \bar{n}$, where $\bar{n}$ is the refractive index of isotropically distributed molecules.

2.2.1. Weak Field Polarization Technique (WFP)

In this technique, the first intense pump pulse is polarized in the z direction and propagates along y, while a second, delayed weak probe pulse, polarized at 45° relative to z, propagates collinearly with the pump, and is analyzed by a cross-polarizer for different pump–probe delays to examine the induced birefringence(Figure 4).

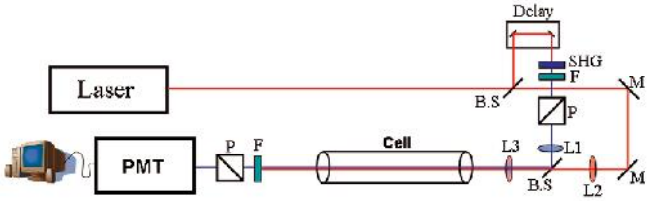

Figure 4. Schematic weak field polarization measurement setup. The fundamental 800 nm laser pulse is split by a beam splitter (B.S.) to a pump pulse (red) and a probe pulse (blue). The probe frequency is doubled by SHG crystal, delayed by a computer-controlled delay line, and is transmitted through the excited cell at varying delays. A filter (F) filters out the fundamental 800 nm. L1, L2, L3 are pump and probe telescopes, sharing a mutual lens (L3).

At times of molecular alignment and anti-alignment ($\Delta n > 0, \Delta n < 0$, respectively), the probe–pulse polarization changes, and when analyzed by the cross-polarizer it yields a homodyne signal measurement. However, a slight rotation of the analyzer off being perpendicular to the probe will result in a small "leak" through it, giving rise to a local oscillator and a heterodyne measurement where the alignment and the anti-alignment peak appear with opposite signs relative to the background signal.

2.2.2. Degenerate FourWave Mixing (or Transient Grating) Technique

Degenerate FourWave Mixing (DFWM) is a nonlinear optical process in which three input electromagnetic fields are coupled by the third order susceptibility $\chi^{(3)}$ to generate a fourth electromagnetic field (the signal). Most of our work here was performed using the time-delayed degenerate forward propagating (Figure 5) three-dimensional phase matched arrangement.[61] An intuitive way of describing DFWM is "transient grating", since two strong fields interfere to create an intensity grating, from which a third (probe) field is Bragg-scattered off. In this picture, two intense short pulses are applied simultaneously at angle, resulting in the formation of a spatially oscillating pattern of the field intensity. During alignment (and anti-alignment) times, and their revivals, the sample develops a refractive index grating, from which the probe field is diffracted off in the phase-matching direction.[61]

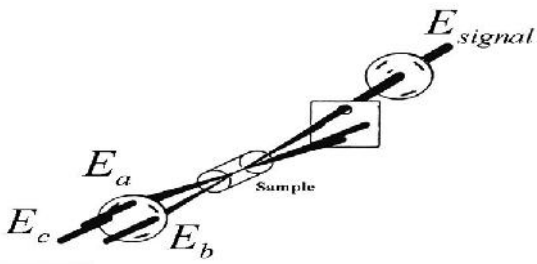

Figure 5. Time-delayed degenerate forward-propagating three-dimensional phase matched four-wave mixing arrangement. The two pump fields E_a, E_b arrive simultaneously, and E_c is delayed. The three fields pass through three corners of a square, and the resulting field E_{signal} is emitted through the forth corner.

As a null detection technique, DFWM is a very sensitive method. In a homodyne measurement, one cannot distinguish between positive and negative changes to the refractive index such as those arising at alignment and anti-alignment times. If a fourth field (local oscillator) is allowed to interfere with the signal beam, one may perform a full heterodyne DFWM measurement.[76]

Typical DFWM and WFP signals from gas-phase nitrogen molecules are depicted in Figure 6 for comparison.

For some of the control schemes presented below two time-delayed interactions (two pairs of excitation pulses) are required. To achieve this, we modified the standard DFWM arrangement as depicted schematically in Figure 7.

2.3. Selective Excitation

2.3.1. Coherent Control of the Rotational Excitation

The first case to be considered here is rotational control by two consecutive pulses. If the second pulse is applied while the molecular ensemble evolves from disk shape to cigar shape (at the full revival time), its effect is similar

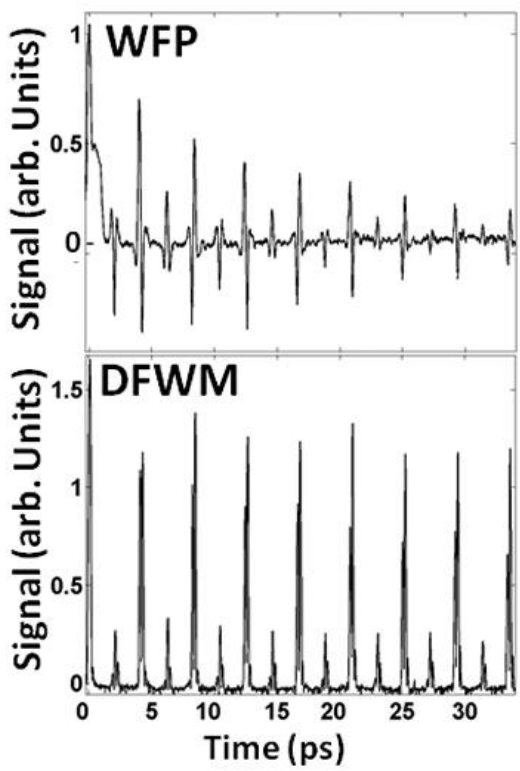

Figure 6. Upper panel: typical Weak Field Polarization (WFP) signal. Lower panel: typical Four Wave Mixing (FWM) signal.

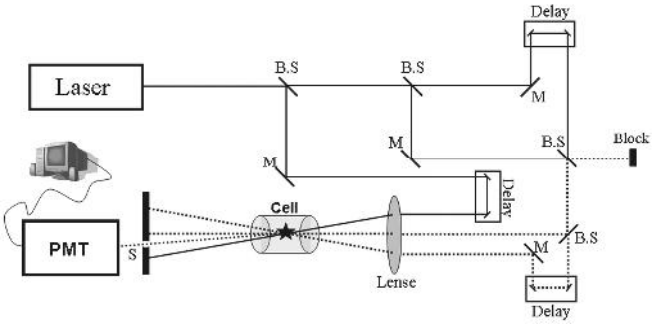

Figure 7. Schematic representation of the FWM optical setup. Two time-delayed pulse pairs (dashed lines) excite the molecular gas. A probe pulse (solid line) is scattered off in the phase-matching direction (dotted line) and recorded by the detector.

to that of the first pulse, namely it kicks the molecules "in phase" with their rotational motion, and adds angular momentum to the already rotating molecules, resulting in higher anisotropic angular distributions. Quantum mechanically, the wavepacket (Equation 2) at $t = T_{rev}$ is identical to the wavepacket at $t = 0$; therefore the molecules are affected by the two pulses delayed by full T_{rev} in exactly the same way. This situation is illustrated in Figure 8a, where the second pulse is applied exactly at $3T_{rev}$: note that the amplitude of the alignment peaks increases significantly.

However, if the second pulse is applied when the molecular angular distribution evolves from cigar shape to disk shape (around the time of half revival), the torque impacted by the second pulse effectively cancels the coordinated motion of the rotating molecules, thwarting any future revivals. Quantum mechanically, the wavepacket at $t = T_{rev}/2$ is π-shifted or "out of phase" with respect to the wavepacket at $t = 0$, as discussed above. This is well illustrated in Figure 8b, where the second pulse was applied at $t = 2^1/_2 T_{rev}$. These conclusions are supported by other experiments in which molecular alignment was observed by weak field polarization technique[77] and by Coulomb explosion imaging.[78]

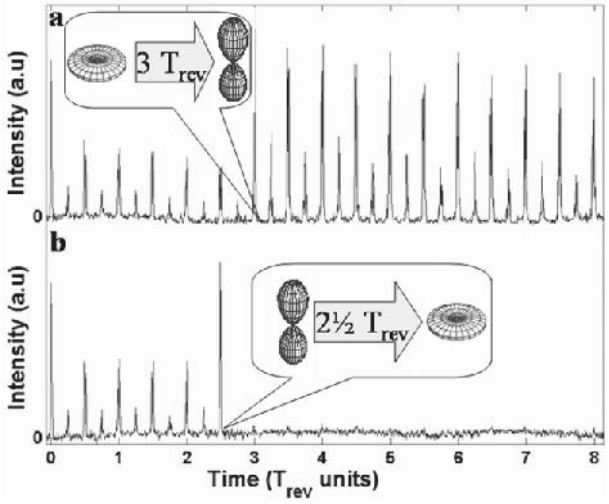

Figure 8. Alignment signal from $^{15}N_2$ gas (300 torr, room temperature), following excitation by two pulses. a) The two pulses are separated by a multiple of the revival time (3 T_{rev}). The torque from the second pulse adds coherently to that from the first one, resulting in the observed enhanced alignment signal. b) The two pulses are separated by an odd multiple of half revival time (2.5 T_{rev}). The torque from the second pulse opposes the molecular angular velocity, resulting in effective stopping of the coherent rotation.

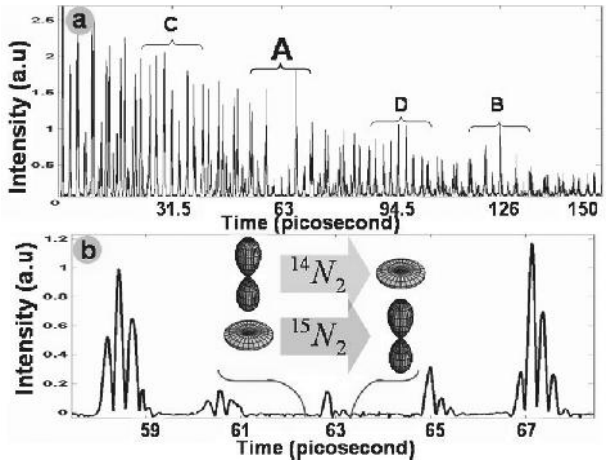

Figure 9. a) FWM signal from 1:1 $^{14}N_2$:$^{15}N_2$ mixture (500 torr, room temperature). Destructive interference of full and half revival signals is seen in region A at ~63 ps. Constructive interference of the two full revival signals is observed in region B at ~126 ps. Interferences of quarter and half revival signals are seen in regions C, D. b) Enlarged view of the destructive interference region A.

2.3.2. Selective Rotational Excitation of Molecular Isotopologues

The control scheme presented here was implemented for the selective excitation of molecular isotopologues in a mixture, demonstrated for the case of nitrogen molecules $^{14}N_2, ^{15}N_2$.

Figure 9a shows a full scan over many revivals of a 1:1 mixture of $^{14}N_2, ^{15}N_2$. The most prominent features are a dip around ~63 ps (region A) and a peak at ~126 ps (region B).

Following the laser pulse excitation (t = 0 in Figure 9a) the molecules start rotating coherently, giving rise to alignment and anti-alignment signals according to their revival periods. Due to their rational mass ratio 14/15, the revival periods ratio of the two isotopologues is rational as well. Thus when the "light" ($^{14}N_2$) molecules complete 15 full revivals, the "heavy" ($^{15}N_2$) molecules complete only 14 full periods, resulting in their constructive contribution to the alignment, as observed at ~126 ps (region B). However, at exactly half of this time, ~63 ps (region A), the two molecular species' contributions to the overall alignment add destructively, as observed by the almost complete cancellation of alignment. Figure 9b depicts the time dependence of the molecular angular distribution

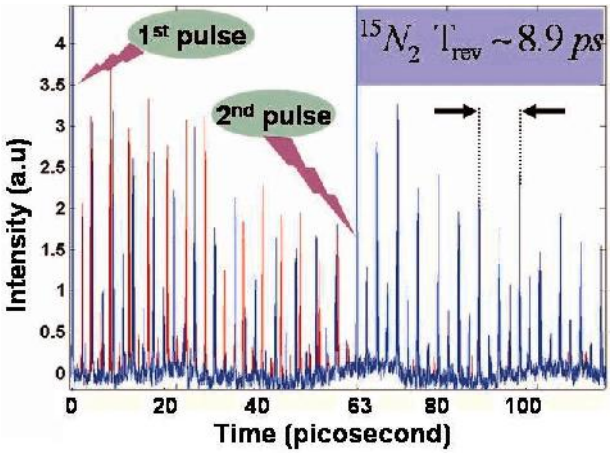

Figure 10. FWM signal from 1:1 mixture of $^{14}N_2$ and $^{15}N_2$ (500 torr, room temperature) subject to two short laser pulses delayed by 63 ps. The first pulse excites both molecular isotopes, but the second pulse affects them in an opposite way, enhancing the coherent rotational motion of $^{15}N_2$ (blue signals) and decreasing the coherent rotational motion of $^{14}N_2$(red signals). As a result, after the second pulse, only the $^{15}N_2$ isotope experiences enhanced temporal alignment as reflected in the periodicity of the signal. The rotational excitation of the second isotope ($^{14}N_2$) is almost completely removed.

separately for the two isotopologues, near the time of ~63 *ps*. A second pulse at that unique time affects the two species very differently. In Figure 10, the second pulse at ~63 ps enhances the alignment of $^{15}N_2$ molecules, and almost completely stops the rotation of $^{14}N_2$ isotopes!

2.3.3. Selective Rotational Excitation of Nuclear Spin Isomers

Linear symmetric molecules whose atomic constituents possess a non-zero nuclear spin exist as either ortho or para spin modifications, differing in the symmetry of their nuclear states. For a homonuclear diatomic molecule with atoms of nuclear spin $^1/_2$, the total nuclear spin can be $I = 1$ (ortho molecule), or $I = 0$ (para molecule). This difference in parity implies statistical differences in the population of even and odd rotational states.[75] Selective excitation of para and ortho isomers is equivalent to selective excitation of even or odd rotational states. In Figure 3, we have already discussed the "out of phase" behavior of the even (Figure 3a) and odd (Figure 3b) rotational manifolds around $^1/_4$ and $^3/_4$ of the revival time, setting the stage for selective manipulation of the two species. Using the same arguments made for the selective excitation of isotopologues, a pulse applied at these unique times affects the two species in the opposite ways, that is, it increases the rotational energy of one of the species while reducing that of the other one.

Figure 11 depicts the calculated dependence of the rotational energy of the even (para) and odd (ortho) states

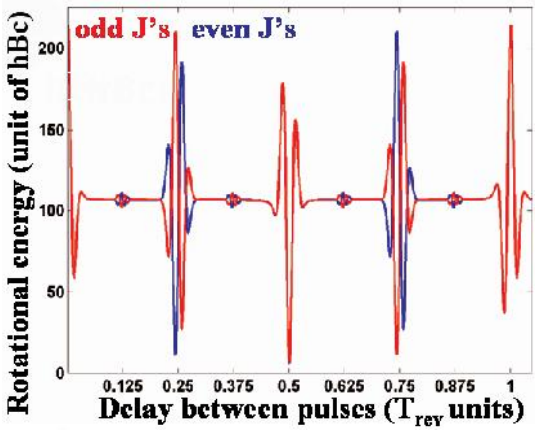

Figure 11. Calculation of the absorbed rotational energy as a function of the time delay between the first and second pulse. Around $^1/_4$and$^3/_4T_{rev}$ the rotational energy content of the odd and even states can be manipulated such that an absorbed energy ratio of ~1/11 is in reach.

separately, as a function of the delay between the first and second pulse. In the vicinity of $^1/_4$ and $^3/_4T_{rev}$ the molecular response is dramatically different, and the two species behave "out of phase" with respect to each other.

Figure 12 depicts the time dependent signal following a two-pulse excitation.

The first pulse (at $t = 0$) excites both para and ortho isomers, which is manifested by the alternation of peak intensities due to the interference of the odd and even manifolds (Figure 12a, 12b in the region $0-1^1/_4\ T_{rev}$). The second pulse, applied just before $1^1/_4\ T_{rev}$ (Figure 12a), gives rise to enhanced alignment signals of almost equal intensity. The absence of the intensity alternation serves as an indication for the purity of a single spin isomer exci-

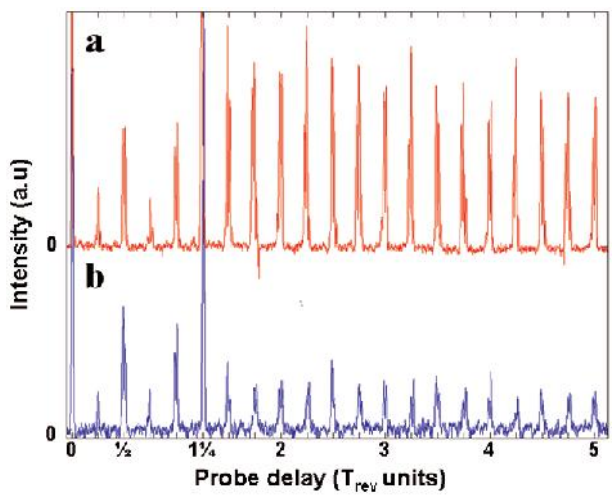

Figure 12. Time domain FWM signal from doubly excited $^{15}N_2$. The second pulse was applied a) just before $1^1/_4\ T_{rev}$, b) just after $1^1/_4\ T_{rev}$.

tation, since only molecules populating the same J parity are excited. When the second pulse is applied just after $1^1/_4\ T_{rev}$ (Figure 12b), the alternation is also removed, indicating pure parity. The ortho-to-para abundance ratio of 3 : 1 explains the reduced intensity when compared to the ortho or the mixed species signal.

The purity of excitation is further verified in the frequency domain. Figure 13b depicts the Fourier transform of the time domain signal in Figure 13a, following the second pulse.

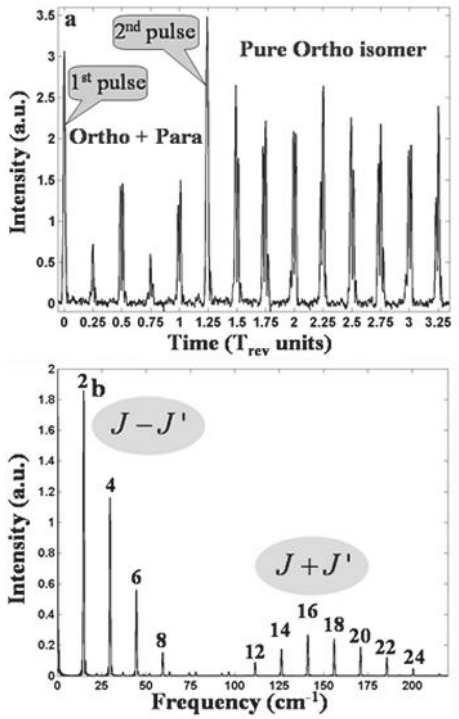

Figure 13. a) Time domain FWM signal of $^{15}N_2$at room temperature following a two-pulse excitation. The first pulse is applied at $t = 0$. The second pulse is applied just before $1^1/_4 T_{rev}$ in order to selectively excite the ortho molecules. b) Fourier transform of the time domain signal in (a), showing that only even sums and differences of J states are excited.

Since DFWM is a nonlinear homodyne measurement, where signal $\propto (\langle\cos^2(\theta)\rangle - 1/3)^2$, its frequency domain shows the sums and differences of the J states. The even binary sums and differences result from J states of the same parity ($even = even \pm even, odd \pm odd$) while the odd binary sums and differences involve J states of different parities ($odd = even \pm odd$); thus the appearance of only even J state combinations (sums and differences) is a manifestation of the selectivity of excitation and the corresponding spin purity (marked in Figure 13b).

3. Controlling the Sense of Molecular Rotation

For single pulse schemes, as well as for techniques using multiple pulses polarized in the same direction, no preferred sense of rotation exists, due to the axial symmetry of the excitation. In order to inject angular momentum into the medium and to force the molecules to rotate with a preferred sense of rotation, one has to break the axial symmetry. This has been previously demonstrated in the "optical centrifuge" experiment by Karczmarek et al.[60] and recently also by Yuan et al.,[79] who used two oppositely chirped, circularly polarized pulses overlapping in time and space, thereby creating a linearly polarized pulse rotating unidirectionally and accelerating in a plane. Recently, we suggested a simple scheme ("molecular propeller") for exciting unidirectional molecular rotation by means of a pair of delayed cross-polarized laser pulses.[6] Pictorially, our double-pulse control scheme is illustrated in Figure 14.

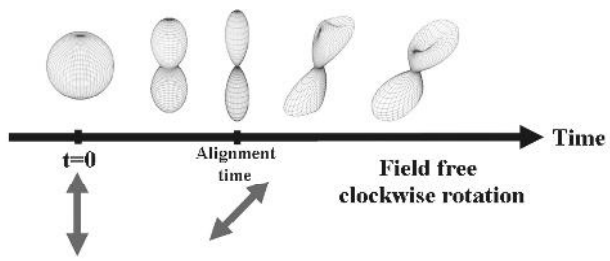

Figure 14. Double-pulse scheme for excitation of unidirectional molecular rotation.

If at the time of maximal alignment (see above) a second pulse, linearly polarized at an angle to the first one, is applied, unidirectional molecular rotation is induced in the sample.

In Figure 15 we present the calculated expectation value of the y-component of the angular momentum $\langle J_y \rangle$ as a function of the polarization angle of a second pulse applied at the time of maximal alignment (marked by an arrow in the inset).

As can be expected, the maximal angular momentum is achieved by two pulses polarized at 45°/−45° with respect to each other.

Varying the time delay between the two pulses (polarized at 45° relative to each other) offers another handle for controlling the unidirectional rotation as depicted in Figure 16.

The sense of rotation depends strongly on the molecular angular distribution at the instant of the second pulse. Following the discussions regarding molecular isotopologues and nuclear spin modifications, one can induce the opposite sense of rotation in different species in the mixture, by correctly choosing the time delay between the pulses, as depicted in Figure 17, where the sense of rota-

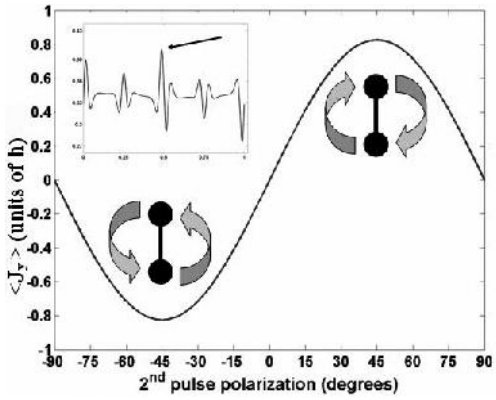

Figure 15. Expectation value of the angular momentum along the *y* axis as a function of the polarization angle of the second pulse. The second pulse is applied at the maximally aligned state, just before $^1/_2T_{rev}$. The direction of the molecular rotation is depicted by the cartoons, showing maximal clockwise and counter-clockwise rotation for 45° and −45°, respectively.

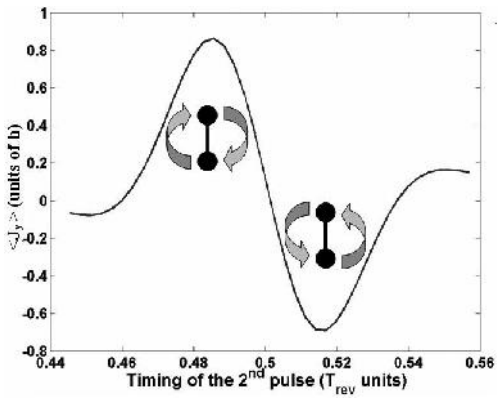

Figure 16. Calculation of the induced angular momentum $\langle J_y \rangle$ as a function of the time delay between the pulses around $^1/_2T_{rev}$.

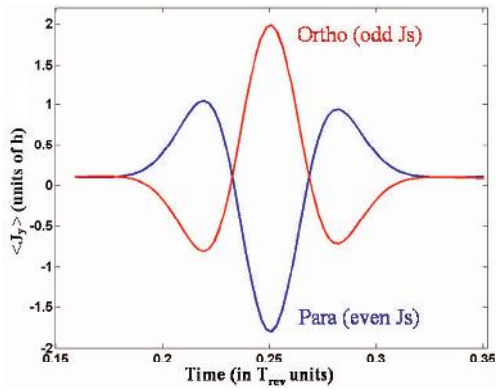

Figure 17. Calculation of the induced angular momentum $\langle J_y \rangle$ as a function of the time delay between the pulses around $^1/_4T_{rev}$, for the ortho (red) and para (blue) spin modifications.

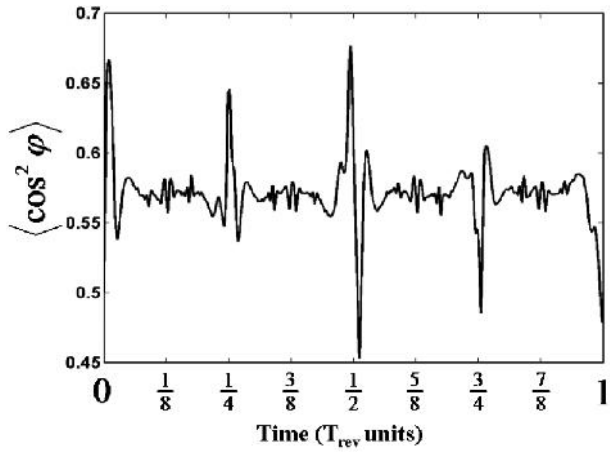

Figure 18. Calculated value of $\langle \cos^2 \varphi \rangle$ as a function of time after the second pulse.

tion is determined by choosing the delay between the pulses to be $^1/_4$ of the revival time.

The introduction of angular momentum along the *y* axis (positive or negative) is equivalent to molecular rotation in a plane perpendicular to *y*. The double-pulse unidirectional excitation scheme results in confinement of the molecular angular distribution to the plane defined by the polarizations of the pulses, namely the *zx* plane.

In order to investigate this non-isotropic molecular motion, we consider a new observable $\langle \cos^2 \varphi \rangle$, correlated with the confinement of molecules to the *zx* plane, where φ is the azimuthal angle. In Figure 18 we plot $\langle \cos^2 \varphi \rangle$ as a function of time. The zero time corresponds to the moment when the second pulse is applied, since prior to the second pulse, $\langle \cos^2 \varphi \rangle = 1/2$, and it is time independent.

The time-averaged value of $\langle \cos^2 \varphi \rangle$ in Figure 18 is ~0.57, which certainly exceeds the isotropic value of 0.5. This means that the molecular axis indeed preferentially occupies the plane defined by the two polarization directions.

Note that the variable $\langle \cos^2 \varphi \rangle$ experiences fractional revivals around $1/3, 1/6, 1/8$ of the full revival time. These are clearly visible in Figure 18, but their origin and methods for their observations will not be discussed in this review.

The first experimental demonstration of a controlled sense of rotation was performed using benzene molecule.[80] Despite its higher complexity, the interaction of benzene with an ultrashort laser pulse is described by the same equation as for the linear molecule, Equation 1. The interaction depends, as before, on the envelope of the electric field squared; on the polarizability anisotropy $\Delta\alpha$, which is negative in the case of benzene; and on the angle between the pulse polarization direction and the molecular symmetry axis. Note that the laser pulse does not influence the rotation around the molecular axis, because of the hexagonal symmetry of the molecule under the rigid rotor approximation.

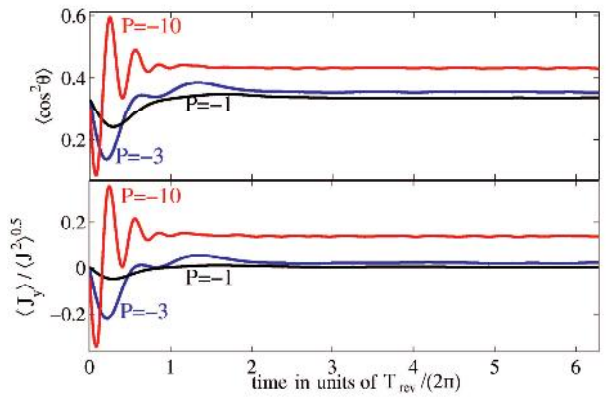

Figure 19. Classical treatment. The upper panel shows the thermally averaged alignment factor $\langle cos^2\,\theta\rangle$ for benzene molecules kicked by the first pulse, plotted as a function of time after the pulse. The pulse strengths used for both pulses are $P=-1,-3,-10$ depicted in black, blue, and red respectively. The first pulse is polarized along the z-axis. The lower panel displays the (normalized) value of the angular momentum orientation $\langle J_y\rangle/\sqrt{\langle J^2\rangle}$ induced by the second pulse, shown as a function of the delay of this pulse. The polarization direction of the second pulse is at -45° degrees to the first pulse. The initial rotational temperature is 0.9 K. The calculations were done using the Monte Carlo method with 10^5 realizations.

In the quantum mechanical description, the rotational eigenstates of symmetric top molecules are given by $|J,K,M\rangle$, where J is the total angular momentum quantum number, M represents the projection of the angular momentum on the laboratory z axis, and K represents its projection on the molecular symmetry axis. The corresponding eigenenergy for the benzene molecule is $E_{J,K}=hBc[J(J+1)-K^2/2]$, where $B=\hbar/(4\pi I_1 c)$, and the revival time of the alignment factor is the same as for linear molecules $T_{rev}=1/(2Bc)$. Here I_1 denotes the moment of inertia with respect to the axis in the plane of the molecule ring.

The scheme operation is practically the same as that of diatomic molecules described in the previous subsection, except for a few details, specific for the benzene molecules. Shortly after the first ultrashort pulse, polarized along the z-axis, the molecules experience a transient anti-alignment, as opposed to alignment in the case of linear molecules. The second pulse, polarized at 45°, drives the anisotropic ensemble to rotate with a preferred sense. The upper panel of Figure 19 presents simulation results for the alignment factor $\langle cos^2\,\theta\rangle$ following the first pulse for three values of the pulse strength, defined as:

$$P=\frac{\Delta\alpha}{4\hbar}\int_{-\infty}^{\infty}E^2(t)dt, \tag{6}$$

where E is the pulse envelope. The lower panel depicts the angular momentum orientation induced via the interaction with two equally strong pulses, polarized at 45° with respect to each other. In the simulations we used the parameters of the benzene molecule:[81] $B=0.190\,\mathrm{cm}^{-1}$, $\alpha_{\parallel}=6.67\,\text{Å}^3$, $\alpha_{\perp}=12.4\,\text{Å}^3$, and an initial rotational temperature of 0.9 K (as in the experiment[80]).

The plots for $\langle cos^2\,\theta\rangle$ show that the anti-alignment becomes more pronounced and occurs at earlier times as the pulse intensity increases. The second pulse is applied at the time of the maximal squeezing of the molecular angular distribution, that is, when the alignment factor reaches its minimal value. In Figure 19, $\langle J_y\rangle/\sqrt{\langle J^2\rangle}$ (calculated after the second pulse) is plotted as a function of the time delay between the first (along the z-axis) and the second pulse (at -45°). Note that the optimal delay becomes shorter with the strength of the pulses.

Figure 20 presents the same quantities, calculated quantum mechanically. On the long-time scale, it demonstrates quantum rotational revivals, such as half and full revivals, that are absent in the classical results in Figure 19. As follows from a comparison between Figure 19 and Figure 20, the rotational dynamics in the vicinity of t = 0 is adequately described by the classical treatment.

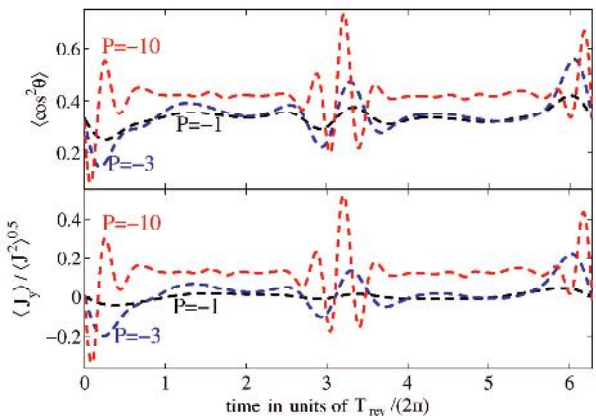

Figure 20. Quantum mechanical calculation of the same quantities as in Figure 19. Half and full rotational revivals are observed (not present in the classical treatment of Figure 19).

The measurement of unidirectionally rotating molecules was performed by the group of Y. Ohshima with benzene molecules in a molecular beam.[81] The molecules were excited by two cross-polarized femtosecond laser pulses, as shown in Figure 21. The delay time between the pulses, corresponding to the time of the first anti-alignment following the first exciting pulse, was chosen to be t = 7.3 ps. The angle between the polarizations of the two pulses was +45° and −45°.

After the excitation by the femtosecond pulses, the excitation spectrum of the benzene molecules was recorded using the resonance-enhanced multiphoton ionization (REMPI) technique. The ionizing probe pulse was circu-

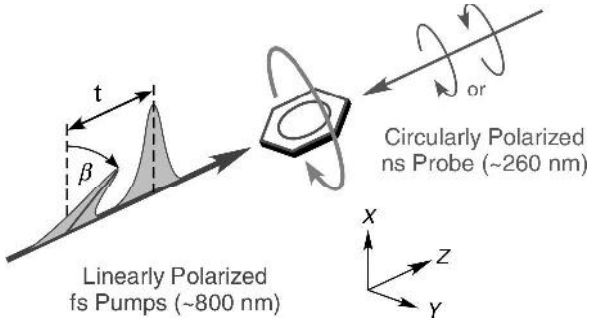

Figure 21. Schematic figure of the experiment in which unidirectional rotation of benzene molecules was induced by two femtosecond laser pulses delayed by a time *t* and cross-polarized at an angle of β. The circularly polarized probe pulse is also shown. (Taken from ref. [80], with permission from the authors.)

larly polarized clockwise or counter-clockwise, as is shown schematically in Figure 21. Molecules rotating in a chosen direction lead to different excitation spectra when the clockwise and the counter-clockwise polarized probes are used, because of angular momentum conservation considerations. The experimental result is shown in the middle pair of curves in Figure 22. The corresponding calculated spectra are reepresented by the dotted lines. By changing the angle between the cross-polarized excitation pulses from -45° to $+45^\circ$, the sense of rotation of the excited benzene molecules is reversed, and leads to the reversed results shown in the lower curves of Figure 22.

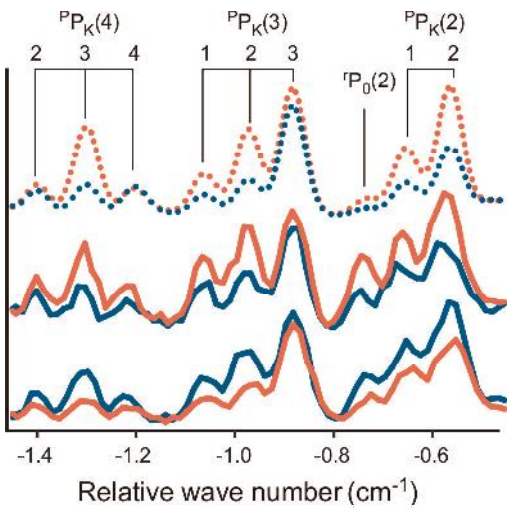

Figure 22. A specific branch of the excitation spectra of benzene molecules following their excitation by two laser pulses, as shown in Figure 21. The spectra were recorded with the clockwise [blue lines] and the counter-clockwise [red lines] polarized probe pulses. The upper (theoretical) and the middle (experimental) panels are for molecular rotation excited with pulses cross-polarized with $\beta = -45^\circ$. A reversed result is seen at the lower panel, where $\beta = +45^\circ$. (Taken from ref. [80], with permission from the authors.)

4. Modifying Molecule–Surface Scattering by Ultrashort Laser Pulses

In this section we explore two schemes for controlling molecule-surface scattering processes, which are based on the laser-induced molecular alignment.

"Laser-kicked" molecules attain the transiently aligned cigar state shortly after the end of the pulse. In addition, at integer and fractional multiples of the rotational revival time this aligned state reappears due to the rotational quantum revivals discussed in Section 2.1. When averaged over time, the angular distribution of the kicked molecules exhibits a net anisotropy and takes the form of a cigar, elongated along the polarization direction of the exciting laser pulse. This means that, in addition to the transient alignment of the kicked molecules, there also exists a permanent alignment of the molecular system, which will be exploited for the control of the molecule-surface scattering process described here.

The permanent net alignment of the molecules can be easily explained for molecules at zero temperature kicked by an ultrashort laser pulse. Consider the orientation of the molecules described by a unit vector directed along the molecular axis. The unit vector will generally trace some trajectory on a surface of a unit sphere. Following the kick applied to non-rotating molecules at zero temperature, all the molecules will trace big circles passing through the "north" and "south" poles of the unit sphere. This leads to a net permanent alignment of the molecular sample, which results, at zero initial rotational temperature, in a time-averaged alignment factor of 1/2. It is important to stress that the permanent alignment effect exist both in the classical and in the quantum descriptions.

4.1. Surface Scattering and Conservation Laws

The model for the molecule-surface scattering process used in this section is a simplified classical model, in which the molecule is treated as a rigid dumbbell. This dumbbell collides with a flat frictionless hard cube, which represents one of the surface atoms. We assume that the cube has some velocity that is distributed according to the surface temperature. This hard-cube model[82,83] provides a simple way of adding surface phonons to the molecule–surface collision process. For the sake of simplicity, we assume that the cube is much heavier than the molecule, so that its velocity does not change as a result of the collision. In this case, by moving to the frame attached to the cube, one reduces the problem to the molecular collision with a hard motionless wall. In the moving coordinate system, the total molecular energy (translational + rotational) is conserved, but it can be redistributed between these two parts as a result of the collision according to the law of conservation of energy:

$$E_{trans,initial} + E_{rot,initial} = E_{trans,final} + E_{rot,final} \quad (7)$$

What about the translational linear momentum of the molecule in the moving coordinate system? The component perpendicular to the surface is not conserved, because the surface exerts forces on the molecule in this direction during the collision. On the other hand, there are no forces applied in the direction parallel to the frictionless surface, and therefore the linear momentum parallel to the surface is conserved.

Using energy and angular momentum conservation laws (for details see ref. [84]), we derive analytic expressions for the translational and the rotational velocities of the dumbbell molecule after the collision. These velocities depend on the velocities before the collision, and on the angle between the dumbbell and the surface of the cube at the moment of collision. Finally, we transform the velocities back to the laboratory coordinate frame.

4.2. Scattering-Induced "Molecular Propeller"

In this subsection we explore a way of inducing unidirectional molecular rotation by a single laser pulse and a surface-scattering event. In Section 3, two time-delayed and cross-polarized laser pulses were used to induce molecular rotation in a preferred sense. Here we achieve a similar goal by replacing the second laser pulse by the process of molecular scattering from a solid surface.

Consider a monoenergetic molecular beam of diatomic molecules flying toward a flat surface at the incidence angle of 45°, as shown in Figure 23. For simplicity, all the molecules have the same velocity vector. Before hitting the surface, the molecules are aligned by a laser pulse polarized at 45° to the surface. Upon their collision with the surface, the aligned molecules receive a "kick" from it and scatter with rotation in a specific direction. By changing the polarization angle of the laser with respect to the surface to −45°, the sense of rotation of the scattered molecules can be inverted. It is important to emphasize, that it is not required that the molecules aligned by the laser pulse hit the surface at some specific time after the aligning pulse. Differently, in the double-pulse scheme of Section 3, the time delay between the two pulses is important.

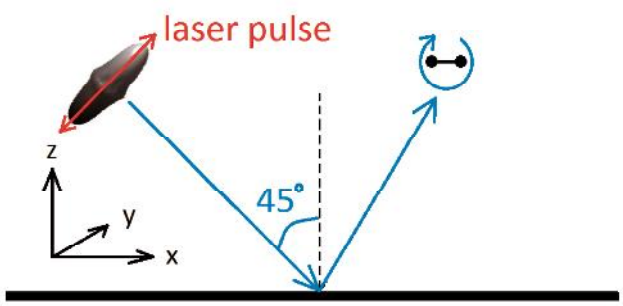

Figure 23. A molecular beam impinges on a hard-wall surface at an angle of 45°. Before hitting the surface, the molecules are "kicked" by an ultrashort laser pulse polarized as shown by the double-headed (red) arrow. This pulse generates the *time-averaged* angular distribution of the molecular orientation in the form of the "cigar" as shown. These aligned molecules are preferentially rotating clockwise after hitting the surface.

After the molecules are "kicked" by the laser pulse, they start rotating in a concerted way, while continuing to approach the surface. The angular distribution of the "kicked" molecules, after averaging over time, is elongated along the pulse polarization direction, as was explained in the beginning of Section 4, and as is depicted schematically in Figure 23 by the cigar-shaped distribution. The result of this time-averaging is the same as that of the averaging along the distance parallel to the direction of the molecular beam propagation. From the above we conclude that *on average* the molecules approaching the surface are aligned along the polarization direction of the ultrashort laser pulse. If the molecules are aligned at 45° with respect to the surface, they have a preferred orientation while colliding with the surface. These molecules receive a "kick" from the surface, resulting in a preferred sense of their rotation, for example, a clockwise rotation in Figure 23. If we plot the distribution of the components of angular momentum of the scattered molecules, we expect to see an asymmetry that is correlated with the polarization direction of the exciting pulse.

In the following, we present the results of a Monte Carlo simulation, according to the above scheme, calculated using 5×10^4 N_2 molecules hitting a flat hard-cube surface at an angle of incidence of 45°. The molecules move with an initial velocity of $V_0 = 350\,\mathrm{m\,sec^{-1}}$, and with a rotational temperature of 1 K, which is typical for molecular beam experiments. They receive a kick with a strength of $P = 10$ from an ultrashort laser pulse, before hitting the surface. We choose the surface to be Ag(111), with the appropriate mass of the representative hard cube, and the surface temperature is taken to be 300 K. We choose the polarization direction of the exciting pulse to be at 45° to the surface, in the xz-plane, as shown in Figure 23.

Figure 24 shows the distribution functions of the angular momentum components J_x, J_y, and J_z after the scattering. On the left set of panels, distribution functions for molecules that were not excited by the laser pulse are shown. The distribution functions on the left set of panels are, in general, narrow, because of the initial low rotational temperature of the molecules. The small background seen for the J_x and J_y distribution (absent at J_z) appears because of the forces in the z-direction, exerted by the surface on the molecules. These forces in the z-direction produce torques that change the angular momenta in the x- and the y- but not in the z-direction. In the right set of panels, distribution functions for molecules that were ex-

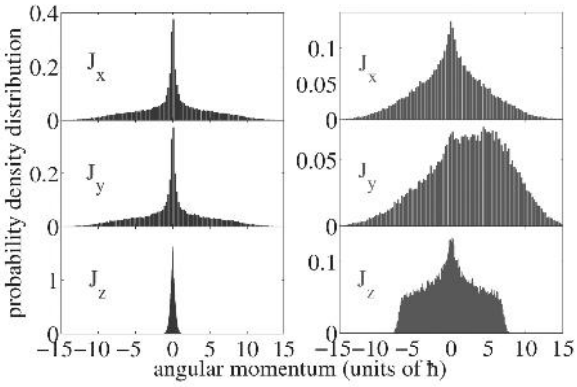

Figure 24. Distribution of angular momentum components J_x, J_y and J_z of the molecules scattered from a hard-cube surface are plotted in the panels. In the right set of panels, the molecules are aligned by an ultrashort laser pulse before they reach the surface, as shown in Figure 23, while in the left set of panels there is no laser excitation prior to their collision with the surface. As expected, the distribution of J_y for laser-excited molecules (on the right set of panels) is asymmetric, and there are more molecules with a positive J_y. The average value of J_y is 2.3 $\hbar$. The calculation is done with the hard-cube model for nitrogen incident with translational velocity of 350 m sec^{-1} and rotational temperature of 1 K. The laser pulse strength is $P = 10$, and the polarization angle is $\gamma_{pol} = 45°$. The surface is composed of silver atoms at room temperature. In this Figure and in Figures 25 and 27 the results of a Monte Carlo simulation of 5×10^4 molecules are shown.

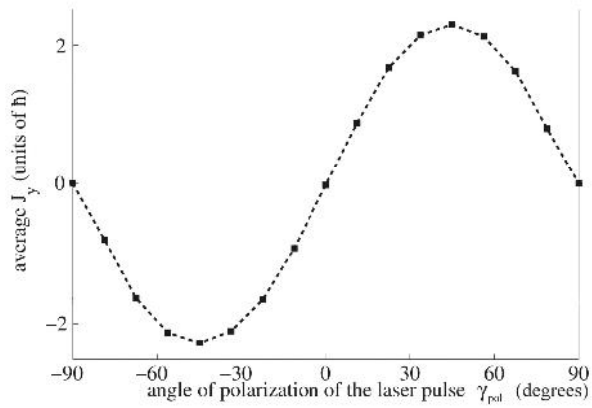

Figure 25. The average induced angular momentum component $\langle J_y \rangle$ is plotted as a function of the polarization angle of the pulse γ_{pol}. The parameters are the same as in Figure 24. The squares represent the results of the simulations, and the lines are shown only to guide the eye.

cited by the laser pulse are shown for comparison. We see that the distributions of J_x and J_z are symmetric around zero, as expected from the symmetry of the pulse. However, most of the molecules are scattered with positive J_y. In addition, the distribution functions on the right set of panels are wider than on the left set because of the angular momentum transferred to the molecules by the laser pulse. The maximum value of J_y in the right middle panel is around $5\hbar$ (notice that $\hbar$ appears only for the purpose of showing the classical results in convenient units).

Switching the polarization direction to $-45°$ inverts the J_y distribution of the scattered molecules, corresponding to negative values of J_y. In Figure 25 we plot the average induced y-component of the angular momentum as a function of the angle of the linear polarization direction of the pulse in the xz-plane. We denote this angle by γ_{pol}, such that a pulse polarized along the z-axis corresponds to $\gamma_{pol} = 0$. It is seen, as expected, that the largest induced $\langle J_y \rangle$ is obtained for a polarization angle close to 45°. Switching the polarization direction to $-45°$ results in the largest induced $|\langle J_y \rangle|$ with an opposite sign. The $\langle J_y \rangle$ dependence on the angle of polarization is similar to the case of the double pulse excitation scheme, depicted in Figure 15.

4.3. Laser-Controlled Surface Scattering of Isotopes and Nuclear Spin Isomers

In this subsection, we show that, in principle, one may use laser-controlled surface scattering for separating molecular beams consisting of several molecular species into individual components. The scheme seems to be applicable to different types of molecular species, such as isotopes, or nuclear spin isomers, and is based on the fact that rotationally excited and unexcited molecules have different scattering angle distributions after collision with the surface.

As an example, we consider a molecular beam composed of a mixture of two nitrogen species. They can be two molecular isotopes, such as $^{14}N_2$ and $^{15}N_2$, or two nuclear spin isomers, such as ortho and para isomers of $^{15}N_2$. It was shown in Section 2.3 that two properly delayed ultrashort laser pulses may selectively align a preferred component of such a mixture, while leaving the other component practically unexcited.

Assume now that such a selectively excited molecular beam hits a solid surface, as shown schematically in Figure 26. For a moment, we also assume that the surface is not vibrating (that is, it stays frozen at zero temperature). According to Equation 7, the rotationally hot (aligned) molecular species, represented by dumbbells with circular ends in Figure 26, have a high probability of transferring their rotational energy to translational energy via the collision. As a result, the perpendicular component of the molecular velocity after the collision is larger than that before the scattering (the parallel velocity component remains the same). In other words, these molecules have a high probability to be scattered to angles smaller than the specular angle (i.e., to "subspecular" angles). The second species, which are rotationally cold (and isotropically oriented) and are represented by

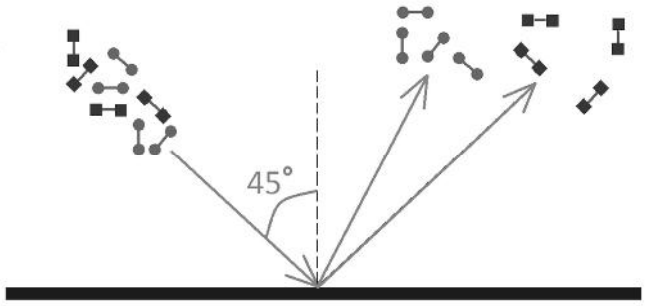

Figure 26. A mixture of two molecular species is manipulated by two properly delayed ultrashort laser pulses before hitting the surface. The species represented by dumbbells with square ends are rotationally cold (their rotation is deexcited by the second laser pulse). The species represented by dumbbells with circular ends are rotationally hot (their rotation was further enhanced by the second laser pulse). After hitting the surface, the "cold" (square-ended) species are mostly scattered specularly, and toward angles larger than the specular angle. On the other hand, the "hot" (round-ended) species mostly transfer their rotational energy to translational energy, and are scattered to angles smaller than the specular angle.

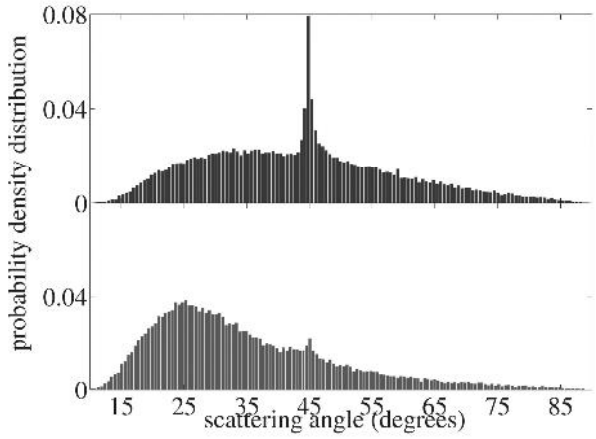

Figure 27. Scattering angle distribution of the "cold" ("square atom") species at the top and the "hot" ("circular atom") species at the bottom, according to the Scheme of Figure 26. The calculation is done using the hard-cube model for nitrogen molecules incident on the surface with translational velocity of 350 m sec^{-1} and rotational temperature of 1 K. The distribution in the top panel is for molecules that are not excited by the laser, representing the species that are deexcited by the second laser pulse. The distribution in the bottom panel is for molecules that are excited by a laser pulse with $P = 10$ and $\gamma_{pol} = 0$. This represents the species that are excited twice by two laser pulses with $P = 5$, with a proper time delay. In the upper panel of the figure, only 52% of the molecules are scattered to subspecular angles, while in the lower panel, 77% are scattered to these angles. This means that almost 50% isotope enrichment may be achieved. The surface cube parameters correspond to silver atoms at room temperature.

dumbbells with square ends in Figure 26, have a high probability for converting their translational energy to rotational energy upon their collision with the surface, and therefore they are mainly scattered to angles larger than the specular angle. As a result of the scattering process, the molecular mixture that arrives to the region of subspecular angles is highly enriched with the "circular atom" species. At finite temperature of the surface, the effect is somehow reduced. The reason is that even a non-rotating molecule can acquire translational energy from a vibrating surface atom moving toward it, and scatter to subspecular angles. However, for a sufficiently strong laser pulse, a significant enrichment is expected even for surfaces at room temperature.

To estimate the magnitude of the effect for typical experimental conditions, we consider the scattering of a beam consisting of a 1:1 mixture of the two nitrogen isotopes discussed above. The beam has an initial translational velocity of 350 m sec^{-1}, a rotational temperature of 1 K, and it propagates at 45° with respect to the surface. The surface consists of silver atoms, and the surface temperature is 300 K. Before hitting the surface, the molecules are excited by a pair of laser pulses of $P = 5$ that are polarized along the z-axis. The timing between the pulses is chosen such that one of the species remains rotationally unexcited, while the other one experiences an effective kick of $P = 10$ from the double pulse, as was explained in Section 2.3. In Figure 27 we plot the distribution of the scattering angles for the two molecular isotopes. The upper panel of this figure corresponds to the unexcited component of the molecular beam, the lower panel corresponds to the selectively excited isotope. In both parts of the figure, the distributions peak around 25–30°, in addition to the specular peak at 45°. The first peak comes from the translational energy delivered to the molecules by the thermally oscillating surface atoms.

Analyzing the distribution functions of Figure 27, we find that 77% of the rotationally hot species are scattered to the subspecular angles, while only 52% of the rotationally cold species are scattered to these angles, which means almost 50% enrichment in the selectively excited isotope. This figure is remarkable by itself; however, it becomes even more impressive at lower surface temperature. The effect is enhanced dramatically for surface temperature below 50 K, and the ratio between the two isotopes asymptotically tends to the impressive value of more than 70 at zero surface temperature. This suggests that cooling the solid surface increases the effect to a large extent.

5. Molecular Deflection in Inhomogenious Fields

5.1. Optical Deflection

In this section we consider the deflection of molecules by inhomogeneous laser field. Although our arguments are rather general, we follow for certainty a deflection

Scheme that brings to mind the experiment by Stapelfeldt et al.[85] who used a strong IR laser to deflect a CS_2 molecular beam, and then addressed a portion of the deflected molecules (at a preselected place and time) by an additional short and narrow ionizing pulse. Consider deflection (in z direction) of a linear molecule moving in x direction with velocity v_x and interacting with a focused nonresonant laser beam that propagates along the y axis (Figure 28).

The spatial profile of the laser electric field in the xz-plane is:

$$E = E_0 exp[-(x^2 + z^2)/\omega_0^2] exp[-2ln2t^2/\tau^2]. \tag{8}$$

The interaction potential of a linear molecule in the laser field is given by Equation 1.

A molecule initially moving along the x direction will acquire a velocity component v_z along the z direction. We consider the perturbation regime corresponding to a small deflection angle, $\gamma \approx v_z/v_x$. We treat z as a fixed impact parameter, and substitute $x = v_x t$. By doing this,

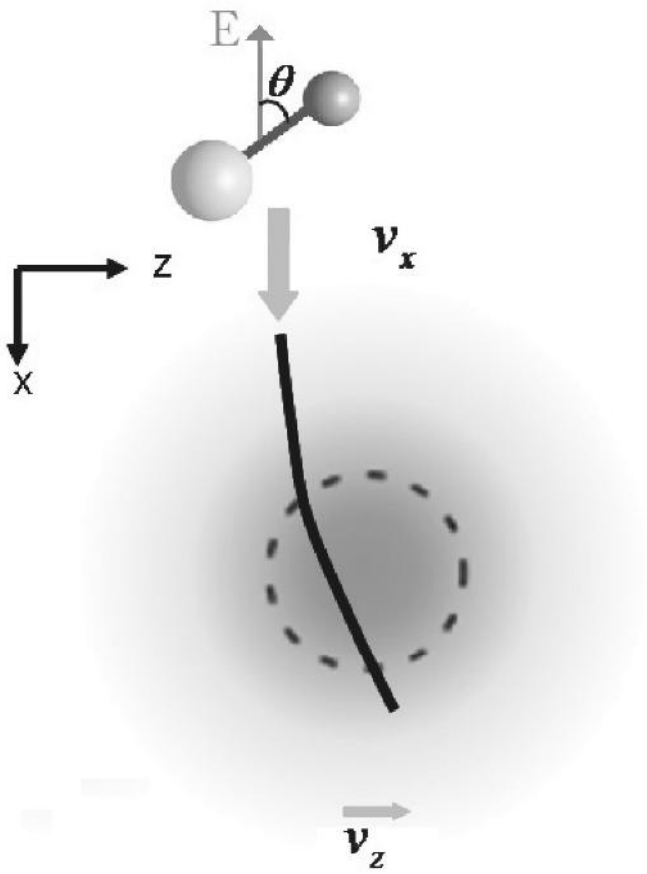

Figure 28. The deflection scheme. A polarized (in the z direction) laser field propagates toward the plane of the paper (y direction). The linear molecules, initially moving along the x direction (with velocity v_x), are deflected by the potential gradient (deflection velocity v_z).

we concentrate on the molecules reaching the focal spot at the moment of the maximum of the deflecting pulse, as in refs. [85,86]. The deflection velocity is given by:

$$v_z = \frac{1}{M}\int_{-\infty}^{\infty} F_z dt = -\frac{1}{M}\int_{-\infty}^{\infty}\left(\vec{\nabla} V\right)_z dt. \tag{9}$$

Here M is the mass of the molecules, and F_z is the deflecting force. The time-dependence of the force F_z (and potential V) in Equation 9 comes from three sources: the pulse envelope, projectile motion of the molecule through the laser focal area, and time variation of the angle θ due to molecular rotation. For simplicity, we consider now the case of the relatively weak deflecting field that does not significantly affect the rotational motion. Such approximation is justified, say for CS_2 molecules with the rotational temperature $T = 5\,\mathrm{K}$, which are subject to the deflecting field of $3 \cdot 10^9 W/cm^2$. The corresponding alignment potential $V \approx -\frac{1}{4}(\alpha_{\parallel} - \alpha_{\perp})E_0^2 \approx 0.04\, meV$ is an order of magnitude smaller than the thermal energy $k_B T$, where k_B is Boltzmann's constant. This assumption is even more valid if the molecules were additionally subject to the aligning pulses prior to deflection. The case of a strong deflecting field will be considered later in this section.

Since the rotational time scale is the shortest one in the problem, we average the force over the fast rotation, and arrive at the following expression for the deflection angle, $\gamma = v_z/v_x$:

$$\gamma = \gamma_0 \left[\alpha_{\parallel} A + \alpha_{\perp}(1 - A)\right]/\overline{\alpha} \tag{10}$$

Here $\overline{\alpha} = 1/3\alpha_{\parallel} + 2/3\alpha_{\perp}$ is the orientation-averaged molecular polarizability, and $A = \overline{cos^2\theta}$ denotes the time-averaged value of $cos^2\theta$. This quantity depends on the relative orientation of the vector of angular momentum and the polarization of the deflecting field. It is different for different molecules of the incident ensemble, which leads to the randomization of the deflection process. The constant γ_0 presents the average deflection angle for an isotropic molecular ensemble:

$$\gamma_0 = \frac{\overline{\alpha} E_0^2}{4Mv_x^2}\left(\frac{-4z}{\omega_0}\right) \times \sqrt{\frac{\pi}{2}}\left(1 + \frac{2\omega_0^2 ln2}{\tau^2 v_x^2}\right)^{-1/2} exp\left(-\frac{2z^2}{\omega_0^2}\right). \tag{11}$$

We provide below some heuristic classical arguments on the anticipated statistical properties of A and γ (both for thermal and prealigned molecules).

Consider a linear molecule that rotates freely in a plane that is perpendicular to the vector $\vec{J}$ of the angular momentum (see Figure 29).

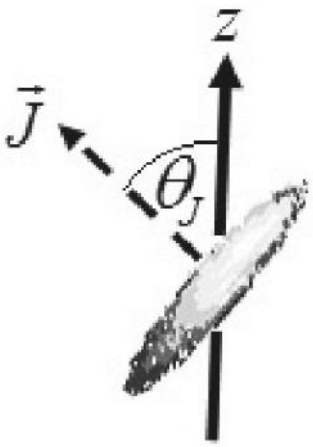

Figure 29. A molecule rotates with the angular momentum $\vec{J}$ forming an angle θ_J with the laboratory z axis.

The projection of the molecular axis on the vertical z-direction is given by:

$$cos\theta(t) = cos(\omega t)sin\theta_J, \tag{12}$$

where θ_J is the angle between $\vec{J}$ and z-axis, and ω is the angular frequency of molecular rotation. By averaging over the time, one arrives at:

$$A = \overline{cos^2\,\theta} = \frac{1}{2}sin^2\,\theta_J. \tag{13}$$

In a thermal ensemble, vector $\vec{J}$ is randomly oriented in space, with isotropic angular distribution density $1/2sin(\theta_J)$. The mean value of the deflection angle is $\langle\gamma\rangle = \gamma_0$. Equation 13 allows us to obtain the distribution function, $f(A)$ for A (and the related deflection angle) from the known isotropic distribution for θ_J. Since the inverse function $\theta_J(A)$ is multivalued, one obtains

$$f(A) = \sum_{i=1}^{2}\frac{1}{2}sin\theta_J^{(i)}\left|\frac{dA}{d\theta_J^{(i)}}\right|^{-1} = \frac{1}{\sqrt{1-2A}}, \tag{14}$$

where we summed over the two branches of $\theta_J(A)$. This formula predicts an *unimodal rainbow* singularity in the distribution of the scattering angles at the maximal value $\gamma = \gamma_0(\alpha_{\|} + \alpha_{\perp})/2\overline{\alpha}$ (for $A = 1/2$), and a flat step near the minimal one $\gamma = \gamma_0\alpha_{\perp}/\overline{\alpha}$ (for $A = 0$).

Assume now that the molecules are prealigned (before entering the deflection zone) by an additional strong, short, and tightly focused laser pulse. The latter is, of course, much shorter than the (nanosecond) deflecting pulse. The arrival time and the location of the focal spot of the aligning pulse are chosen such that the aligned molecules reach the center of the deflection zone at $t = 0$ (that is, at the maximum of the deflecting pulse).

We consider the case where the molecules are prealigned by a short strong laser pulse that is polarized parallel to the direction of the deflecting field. After excitation by such a pulse, the vector of the angular momentum of the molecules is preferentially confined to the xy-plane, and the angle θ_J takes a well-defined value of $\theta_J \approx \pi/2$, which corresponds to $A = 1/2$. In this way, the molecules experience the maximum possible time-averaged deflecting force which is the same for all the particles of the ensemble. As a result, the dispersion of the scattering angles is reduced dramatically. The distribution of the deflection angle γ transforms to a narrow peak (asymptotically — a δ-function) near the maximal value, $\gamma = \gamma_0(\alpha_{\|} + \alpha_{\perp})/2\overline{\alpha}$.

For a more quantitative treatment, involving analysis of the relative role of the quantum and thermal effects on one hand, and the strength of the prealigning pulses on the other hand, we consider quantum-mechanically the deflection of a linear molecule described by the Hamiltonian:

$$H = \hat{J}^2/(2I). \tag{15}$$

Here $\hat{J}$ is operator of angular momentum, and I is the moment of inertia. Assuming again that the deflecting field is too weak to modify molecular alignment, we consider scattering in different $|J,m\rangle$ states independently. The deflection angle is given by Equation 10, in which A is replaced by

$$A_{J,m} = \langle J,m|\,cos^2\,\theta|J,m\rangle = \frac{1}{3} + \frac{2}{3}\frac{J(J+1) - 3m^2}{(2J+3)(2J-1)}. \tag{16}$$

In the quantum case, the continuous distribution of the angles γ is replaced by a set of discrete lines, each of them weighted by the population of the state $|J,m\rangle$. Figure 30 shows the distribution of $A_{J,m}$ in the thermal case for various values of the dimensionless parameter $J_T = \sqrt{k_BT/(hBc)}$ that represents the typical "thermal" value of J (for $J_T \geq 1$). For CS_2 molecules, the values of $J_T = 5, 15$ correspond to T=3.9 K and T=35 K, respectively.

The distribution of discrete values of $A_{J,m}$ demonstrates a non-trivial pattern. In particular, the values exceeding the classical limit 0.5 correspond to the states $|J,m=0\rangle$ (see Equation 16), and they rapidly approach that limit as J grows. After the coarse-grained averaging, however, the distribution shows the expected unimodal rainbow feature (see Equation 14) for large enough J_T.

If the molecules are subject to a strong femtosecond prealigning pulse, the corresponding interaction potential is given by Equation 1, in which E is the envelope of the femtosecond pulse. If the pulse is short compared to the

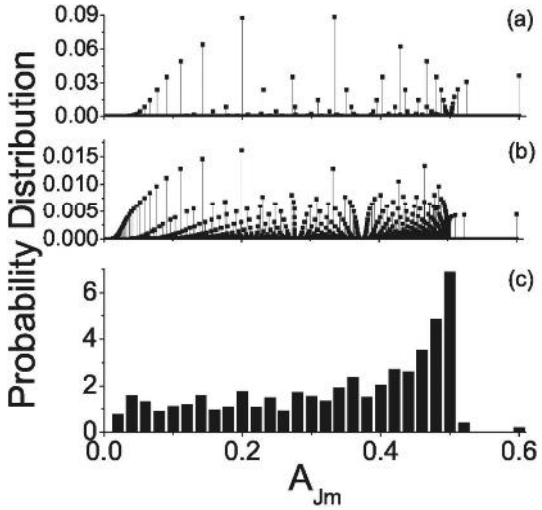

Figure 30. Quantum distribution of $A_{J,m}$ in the thermal case. Panels (a) and (b) correspond to $J_T = 5$ and $J_T = 15$, respectively. Histogram in panel (c) shows a coarse-grained version of the distribution in panel (b).

typical periods of molecular rotation, it may be considered as a delta-pulse. In the impulsive approximation, one obtains the following relation between the angular wavefunction before and after the pulse applied at $t = 0$ (see, e.g., ref. [87] and references therein):

$$\Psi(t = 0^+) = exp(iP\,cos^2\,\theta)\Psi(t = 0^-), \tag{17}$$

where the kick strength, P, is given by Equation 6.

Here we assumed the vertical polarization (along z-axis) of the pulse. Physically, the dimensionless kick strength, P, equals to the typical amount of angular momentum (in the units of $\hbar$) supplied by the pulse to the molecule. For example, in the case of CS_2 molecules, the values of $P = 5, 25$ correspond to the excitation by 0.5 ps (FWHM) laser pulses with the maximal intensity of $4.6{\cdot}10^{11}$ W cm^{-2} and $2.3{\cdot}10^{12}$ W cm^{-2}, respectively. For the vertical polarization of the laser field, m is a conserved quantum number. This allows us to consider the excitation of the states with different initial m values separately. In order to find $\Psi(t = 0^+)$ for any initial state, we introduce an artificial parameter ξ that will be assigned the value $\xi = 1$ at the end of the calculations, and define

$$\Psi_\xi = exp\left[(iP\,cos^2\,\theta)\xi\right]\Psi(t = 0^-) = \sum_J c_J(\xi)|J, m\rangle. \tag{18}$$

By differentiating both sides of Equation 18 with respect to ξ, we obtain the following set of differential equations for the coefficients c_J:

$$\dot{c}_{J'} = iP\sum_J c_J\langle J', m|\,cos^2\,\theta|J, m\rangle, \tag{19}$$

where $\dot{c} = dc/d\xi$. The diagonal matrix elements in Equation 19 are given by Equation 16, the off-diagonal ones can be found using recurrence relations for the spherical harmonics.[73] Since $\Psi_{\xi=0} = \Psi(t = 0^-)$ and $\Psi_{\xi=1} = \Psi(t = 0^+)$ (see Equation 18), we solve this set of equations numerically from $\xi = 0$ to $\xi = 1$, and find $\Psi(t = 0^+)$. In order to consider the effect of the field-free alignment at thermal conditions, we repeated this procedure for every initial $|J_0, m_0\rangle$ state. To find the modified population of the $|J, m\rangle$ states, the corresponding contributions from different initial states were summed together weighted with the Boltzmann's statistical factors:

$$f(A_{J,m_0}) = \sum_{J_0,\bar{J}} \frac{exp(-E^{J_0}/k_B T)}{Q_{rot}} \times|c_{\bar{J}}|^2\delta(A_{J,m_0}, A_{\bar{J},m_0}), \tag{20}$$

where c_J are the coefficients (from Equation 19) of the wave packet that was excited from the initial state $|J_0, m_0\rangle$; δ is the Kronecker delta, and Q_{rot} is the rotational partition function. It worth mentioning that different combinations of J and m may correspond to the same value of $A_{J,m}$, which necessitates the presence of the Kronecker delta in Equation 20. For symmetric molecules, statistical spin factor should be taken into account. For example, for CS_2 molecules in the ground electronic and vibrational state, only even J values are allowed due to the permutation symmetry for the exchange of two bosonic sulfur atoms (which have nuclear spin 0).

Using this technique, we considered deflection of initially thermal molecules that were prealigned with the help of a short pulse polarized in z direction (Figure 31). For strong enough kicks ($P \gg 1$ and $P \gg J_T$), prealignment in the direction parallel to the deflecting field allows for almost complete removal of the rotational broadening. A considerable narrowing of the distribution can be seen when comparing Figure 30 a and Figures 31 b and d. The conditions required for the considerable narrowing shown at Figure 31 d correspond to the maximal degree of field-free pre-alighment $\langle cos^2\,\theta\rangle_{max} = 0.7$. This can be readily achieved with the current experimental technology, even at room temperature.[56]

So far, we found a good correspondence between the classical heuristic considerations and the quantum mechanical calculations.[8,88] Motivated by this correspondence, we will consider now a deflection by a strong field and, for simplicity, provide only classical analysis. In the case of a strong deflecting field, the rotational motion of the molecules may be disturbed by the field.[8,88] Since molecules experience a time-varying amplitude of the optical field while propagating through the deflecting beam,

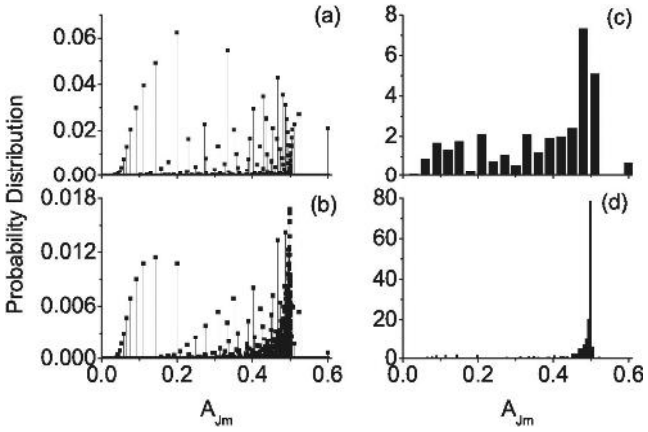

Figure 31. Distribution of $A_{J,m}$ for molecules prealigned in the z direction. The left column (a–b) presents directly the $A_{J,m}$ values, while the right column (c–d) shows the corresponding coarse-grained histograms. Panels (a) and (c) are calculated for $J_T = 5$ and $P = 5$; (b) and (d), for $J_T = 5$ and $P = 25$.

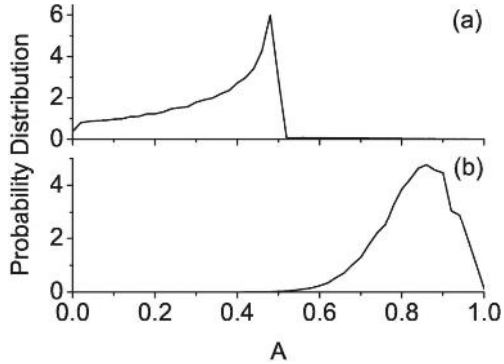

Figure 32. Distribution of A at the peak of the deflecting field. Two cases are considered: (a) weak deflecting field $3{\cdot}10^9\,\mathrm{W\,cm^{-2}}$ and (b) strong deflecting field $9{\cdot}10^{11}\,\mathrm{W\,cm^{-2}}$. In (a) we observe the unimodal-rainbow distribution. In (b), the effect of the alignment by the deflecting field is evident.

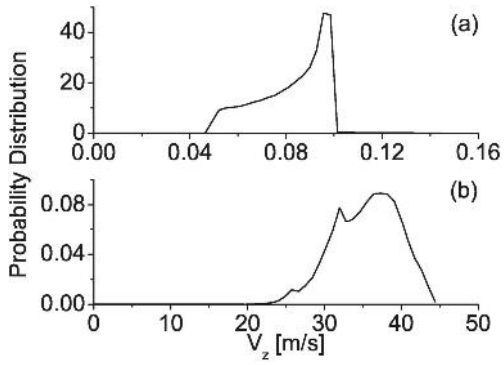

Figure 33. Distribution of velocities (or deflecting angles) calculated from the trajectories of the molecules subject to weak (a) and strong (b) deflecting fields. The fields characteristics are given in the text.

the total rotational energy of the system is changed with time. However, this change is adiabatic with respect to the rotational motion, and therefore we can use adiabatic invariants to determine the energy of the system.[89–91] To illustrate the performance of the procedure under real experimental conditions,[85,86] we consider the deflection of CS_2 molecules at $T = 5\,\mathrm{K}$ (see Figure 28), and plot the distribution of A at the peak of the deflecting field (for more details about the thermal distribution, see refs. [8,88]). The results are given in Figures 32 a and b, for weak ($3{\cdot}10^9\,\mathrm{W\,cm^{-2}}$) and strong ($9{\cdot}10^{11}\,\mathrm{W\,cm^{-2}}$) deflecting fields, respectively.

In the case of a weak field, we get the unimodular rainbow distribution discussed previously. In the case of a strong field we obtain a rotationally-trapped distribution, corresponding to the pendular-like motion of the molecules at the top of the deflecting pulse.[86] To study the deflection of CS_2 molecules by a focused laser beam, we integrate numerically Equation 9 to find the deflection velocity. In the integrand of Equation 9, we substitute the value of $\langle cos^2\,\theta\rangle$ calculated in every point of time. As was previously assumed, $x \approx v_x t$ ($v_x = 500\,\mathrm{m\,sec^{-1}}$) and z is a fixed impact parameter ($z = -4\,\mu\mathrm{m}$). These assumptions are valid even for strong deflecting fields (that align the molecules) since the deflection angle is still small. We consider both weak and strong deflecting fields, as in Figure 32, and use the values of $\omega_0 = 7\,\mu\mathrm{m}$ and $\tau = 14\,\mathrm{ns}$ (Equation 8) in the calculation of the trajectories. The distribution of deflected velocities for a thermal molecular ensemble (without prealignment) is shown in Figure 33.

In Figure 33 a (weak field) we essentially verify our previous assumption that the deflection in weak fields is linear with A (Equation 10). This is seen by observing that Figure 33 a may be indeed obtained by a linear transformation of the distribution $f(A)$ from Figure 32 a. In Figure 33 b(strong field) the distribution of deflection angles (or of deflection velocities) is still quite broad. In our opinion, this results from two different regimes of scattering that the molecules experience while traversing the deflecting beam: weak deflection at the periphery of the beam, and deflection under partial alignment of the molecular ensemble in the center of the beam.

Finally, we consider scattering of molecules prealigned in the z direction with the pulses having kick strength of $P = 25$. The results are given in Figures 34 a and b for weak and strong deflecting fields, respectively. In the case of weak deflection (Figure 34 a), the narrow peak is observed whose nature was already explained above. More interestingly, the distribution of the deflection angles regained the narrow shape even in the case of strong deflection field (Figure 34 b) as a result of prealignment. In our example, the prealignment pulse was strong enough to overcome the rotational trapping by the deflecting field. As a result, all the molecules performed full rotations (but not a pendular motion) despite the presence of the

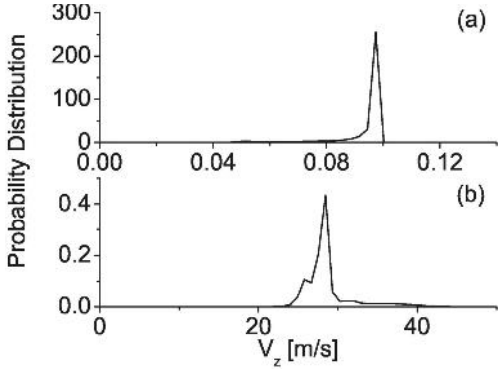

Figure 34. Distribution of deflection velocities for prealigned molecules ($P = 25$). Case (a) is for weak deflecting field, and case (b) is for strong deflecting field. In both cases the molecules were prealigned parallel to the deflecting field, and this prealignment was strong enough to ignore any aligning effect of the deflecting field (thus reducing the broadening of the deflection, as explained in the text).

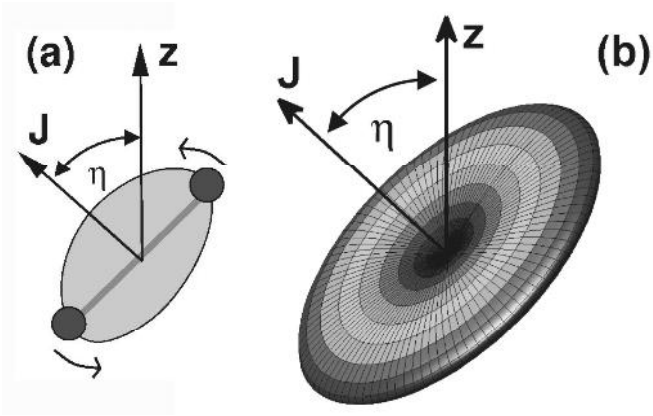

Figure 35. (a) A classical molecule rotates in the plane perpendicular to its angular momentum **J**. (b) Disc-like angular distribution for the tilted spinning state $|J, J\rangle_\eta$ with $J = 25$. The state is almost confined to a plane, as in the classical case (a).

strong deflecting field, and we obtain a narrow distribution as well.

5.2. Molecular Frisbee

In a thermal ensemble of rotating molecules the orientation of individual molecules, as well as the orientation of their vector of angular momentum, is completely random. In the recent years several studies addressed the challenge of the optical preparation of molecules in a highly-spinning state[6,60,80,92–95] with a well-defined direction of the vector of angular momentum. At least two routes leading to this goal have been demonstrated experimentally, including the "optical molecular centrifuge",[60,92,93] where the molecules are angularly accelerated by a laser field with a spinning polarization vector, and the "molecular propeller" technique,[6,80,94] which uses two time-delayed cross-polarized short laser pulses.

The molecular axis of the fast-spinning molecules is confined to the rotation plane perpendicular to the vector of the angular momentum, and the molecular angular distribution has a specific disc-like shape (see Figure 35). In this section we consider deflection of the spinning molecules by inhomogeneous fields, and show that the trajectories of these "flying discs" may be controlled and fine-tuned by inclination of the plane of laser-induced rotation with respect to the external fields. A similar technique is used by Frisbee players finessing the tilt of the spinning disc for directing it into a pair of waiting hands.

We will concentrate, as before, on the molecular deflection by optical fields, which is a hot experimental subject,[85,96,97] although similar arguments are applicable to the scattering in static fields as well. In the previous section we showed how the scattering distribution of the molecules may be narrowed by prealignment. In this section we show that if the molecules are prepared in the fast-spinning state, not only they are scattered into a narrow angular interval, but also the position of this scattering peak is fully controllable by ultra-fast lasers.

For certainty, we follow the deflection scheme from Section 5.1. For simplicity, we assume also that the deflecting field does not significantly affect the rotational motion. Such an approximation is justified, say for CS_2 molecules in a rotational state with $J = 30$, which are subject to a deflecting field of $5{\cdot}10^{11}\,\mathrm{W\,cm^{-2}}$. As in Section 5.1, we consider the time-averaged value of $cos^2\theta$, which is given by Equation 13. Substituting η instead of θ_J (See Figure 35) in Equation 13, one arrives at

$$A = \overline{cos^2\theta} = \frac{1}{2} sin^2\eta. \tag{21}$$

The thermal distribution of A was already given in Section 5.1. However, for fast-spinning molecules the distribution of **J** is completely different, as **J** is mostly perpendicular to the well-defined molecular plane of rotation (in this section the angular momentum vector $\vec{J}$ is denoted by **J**). Classically, the angle η takes a well-defined value, and we expect the distribution of A to be very narrow (delta-function) and, more importantly, to be centered around the value determined by η. By tuning the inclination of the plane of rotation, the scattering angle can be continuously varied.

Quantum mechanics, however, limits the accuracy by which the angular momentum can be oriented along a given direction. Quantum states which assign a particular direction to the vector **J** with minimal uncertainty were introduced in the context of quantum optics and called directional-angular-momentum states,[98] or atomic coherent states (Bloch states).[99] In the case of rotating linear molecules, the directional-angular-momentum state is a tilted spinning state $|J, m = J\rangle_\eta$, where J is the angular momentum quantum number and m is the quantum

number associated with the projection of angular momentum on the tilted **J** direction (see Figure 35b). The angular distribution for a molecule in the $|J=25, m=25\rangle_\eta$ state is plotted in Figure 35b, where we observe that the molecule is mostly confined to the plane perpendicular to the direction of **J**. The generation of such a state is feasible, for example, by the optical centrifuge approach,[60,92,93] hexapole selection,[100] or selection by deflection.[101] Although the projection of **J** onto the tilted direction is well defined for the $|J,J\rangle_\eta$ state, the projection of **J** along the field polarization is somehow uncertain due to noncommutativity of the different components of angular momentum. This quantum uncertainty leads to the broadening of the deflection peak. To obtain the distribution of deflection angles for a molecule being in such a state, we expand $|J,J\rangle_\eta$ in the basis of $|J,m\rangle$ states with the quantization axis parallel to the deflecting field. This is essentially obtained by rotating the state by the angle η (see Figure 35b):

$$|\Psi\rangle = \hat{R}(\eta)|J,J\rangle_\eta = \sum_{m=-J}^{+J} c_{J,m}|J,m\rangle \ , \tag{22}$$

where $\hat{R}(\eta)$ is the rotation matrix.[102] The expansion coefficients $c_{J,m}$ are given by[103]

$$c_{J,m} = \sqrt{\binom{2J}{J-m}}\left(cos\frac{\eta}{2}\right)^{J+m}\left(-sin\frac{\eta}{2}\right)^{J-m}. \tag{23}$$

For a weak enough deflecting field, the scattering angle for a molecule in the $|J,m\rangle$ rotational state is given by Equation 10, in which A is replaced by $A_{J,m}$ from Equation 16. Figure 36 shows the distribution of $A_{J,m}$ values weighted by the population $|c_{J,m}|^2$ of each state (for several values of η). Using Equation 23, one can show that the distribution of $A_{J,m}$ takes the following form in the limit of $J \gg 1$:

$$f(A) = \frac{1}{\sqrt{2\pi\sigma^2}}\frac{1}{\sqrt{1-2A}} \times \sum_{i=1,2} exp\left[-\frac{\left(cos\eta + (-1)^i\sqrt{1-2A}\right)^2}{2\sigma^2}\right], \tag{24}$$

with $\sigma = |sin\eta|/\sqrt{2J}$. The maximum of the distribution is located near $A_{max} = 1/2\, sin^2\eta$, which is exactly the classical value for A (see Equation 21). The "quantum" width of the corresponding scattering peak tends to zero with increase of J, that is, in the classical limit.

To analyze the experimental feasibility of the suggested control scheme, we consider optical deflection of unidirectionally rotating molecules prepared by the double-pulse "molecular propeller" technique,[6,80,94] as was presented in Section 3. Motivated by the success so far in predicting the main results classically, we provide here only classical calculations. Let us recall briefly the corresponding scenario for inducing molecular spinning (a detailed discussion of this scenario can be found in refs. [6,7,104]). The first short linearly polarized laser pulse (with the polarization vector $\mathbf{p}_1$) brings molecules to a concerted rotation that results in molecular alignment along the $\mathbf{p}_1$-direction sometime after the end of the pulse (in other words, at field-free conditions). At the moment of maximal alignment, when the molecular angular distribution is mostly confined in a narrow cone around $\mathbf{p}_1$, the second, delayed laser pulse is applied, with the polarization vector $\mathbf{p}_2$ at 45° with respect to the first one. As a result, the molecules gain an angular momentum in the $\mathbf{p}_1 \times \mathbf{p}_2$ direction, and start spinning in the plane spanned by the vectors $\mathbf{p}_1$ and $\mathbf{p}_2$.

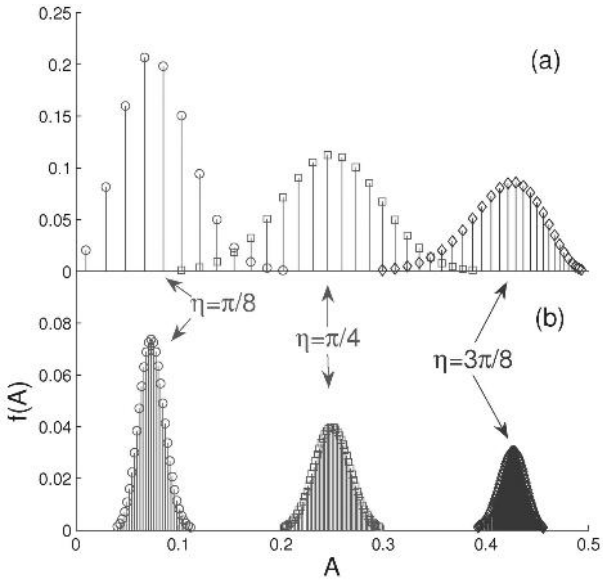

Figure 36. (a) Distribution of A for a $|J,J\rangle_\eta$ state with $J=50$ and different angles η between **J** and the deflecting field. (b) Same as (a) but for $J=400$.

We performed Monte Carlo simulations for a thermal molecular ensemble excited by the above double-pulse sequence for various orientations of the plane of induced spinning with respect to the deflecting field. Since the needed laser pulses are much shorter than the rotational time-scale, we treated them as δ-kicks. After calculating the final value of **J** for every molecule after the two pulses, we obtained A from Equation 21 by using $sin^2\eta = 1-(\mathbf{J}\cdot\mathbf{d})^2/J^2$, where **d** is the unit vector along the deflecting field. The resulting distribution of A is shown in Figure 37 for various values of the angle η.

The parameters of the presented simulation are $P_1 = 10$, $P_2 = 50$, and $J_T = 5$. Figure 37 clearly shows that compact deflection peaks with a tunable position are indeed formed, as predicted above. The distribution ele-

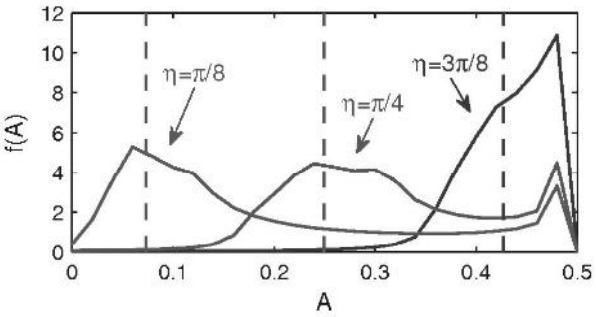

Figure 37. Distribution of $A = \overline{cos^2\,\theta}$ for a classical thermal ensemble of molecules ($J_T = 5$) on a coarse-grained grid. The molecules are excited by two delayed laser pulses cross-polarized at 45° with respect to each other. The kick-strengths of the pulses are $P_1 = 10$ and $P_2 = 50$. The dashed lines show positions of the expected distribution maxima for the molecules perfectly confined to the desired plane of rotation (see Equation 21).

vation near $A = 0.5$ is due to an integrable singularity, which is caused by a residual fraction of molecules with η close to $\pi/2$ because of the non-perfect confinement of the molecules to the rotation plane. To show the distribution of A unobstructed by this singularity, we used a coarse-grained bin averaging in Figure 37. Our results demonstrate that the predicted effect is clearly observable using a rather basic double-pulse scheme for spinning molecules,[6,80,94] which was demonstrated in a recent experiment.[80] An even better outcome can be achieved by the optical centrifuge approach,[60,92,93] which has the potential for generating clean $|J,J\rangle$ states. A recent proposal[95] for generating the coherent superposition $1/\sqrt{2}(|J,J\rangle + |J,-J\rangle)$ with the help of properly shaped perpendicularly polarized laser fields is instrumental for our purposes as well.

The deflection of molecules may occur also in static electric and magnetic fields. In the case of static fields, permanent dipoles (either electric or magnetic) contribute to the interaction (in addition to the polarizability interaction from Equation 1 that has been considered throughly in this review). Those interactions may also be strongly controlled by means of laser-induced field-free alignment. Details about the static field interactions and the ability to control them by means of laser-induced field-free alignment are beyond the scope of this work. For more information on the deflection of linear molecules by a static electric field we refer the reader to ref. [9]. For more information on the deflection by a magnetic field see ref. [105]. Symmetric- and asymmetric-top molecules may exhibit a different behavior throughout the deflection process, and more details about this can be found in ref. [106].

6. Summary and Conclusions

In the present paper we overviewed some recent theoretical and experimental developments related to the control of molecular rotation and orientation in space by means of femtosecond laser pulses. We gave a brief introduction to the basic physics of field-free (nonadiabatic) molecular alignment both from the classical and quantum-mechanical points of view. We also presented a short outline of the experimental techniques used for observing and detecting field-free molecular alignment, with an emphasis on our method of choice, time-delayed degenerate four wave mixing. This introductory part, while not geared to provide a comprehensive review of the literature, reflects the pool of ideas and concepts shared by our research team. We then demonstrated several examples of coherent rotational control in molecular mixtures of species with close chemical and physical properties. In particular, we realized selective alignment of an individual isotopologue in a mixture of $^{14}N_2$ and $^{15}N_2$ molecules, and also performed selective alignment of specific nuclear spin modifications of $^{15}N_2$ species that exist in the form of ortho- and para-isomers. By inducing dramatic differences in the angular distribution of various components of the mixture, one paves the way to futher separation of the aligned species, or their enhanced detection and discrimination.

As a natural advance towards these goals, we explored the prospects of controlling the motion of rotationally aligned molecules in various inhomogeneous fields — electric, magnetic, and optical. In particular, we showed that by preshaping the molecular angular distribution with the help of strong femtosecond laser pulses, one may efficiently control the scattering process in external fields, manipulate the average deflection angle and its distribution, and substantially reduce the angular dispersion of the deflected molecules. As a special example of the rotational control, we suggested a method for inducing unidirectional molecular rotation by cross-polarized time-delayed laser pulses, and demonstrated that the trajectories of spinning molecules in external fields are well controlled by the tilt of the plane of induced rotation with respect to the field and its gradient (a Frisbee-like mechanism). The possibility of such ultrafast optical control over molecular motion opens new pathways for applications involving molecular focusing, guiding, and trapping by optical and static fields. Moreover, we demostrated that the same pool of ideas can be applied to the control of molecular scattering from solid surfaces. We applied this methodology to the selective manipulations of surface scattering of mixed molecular beams (composed of various isotopologues, or spin modifications) and defined conditions for their optimal separation.

The field of ultrafast coherent control of molecular rotation and orientation in space is thriving, with new ideas and applications appearing constantly. We hope the pres-

ent review will give the reader a glimpse at this research area through the prism of our own research experience.

Acknowledgments

Financial support of this research by the Israel Science Foundation and the Deutsche Forschungsgemeinschaft is gratefully acknowledged. YP is an incumbent of the Sherman Professorial Chair. IA is an incumbent of the Patricia Elman Bildner Professorial Chair. This research is made possible in part by the historic generosity of the Harold Perlman Family.

References

[1] For an early review, see B. Friedrich, D. P. Pulman, D. B. Herschbach, *J. Phys. Chem.* **1991**, *95*, 8118.
[2] H. Stapelfeldt, T. Seideman, *Rev. Mod. Phys.* **2003**, *75*, 543.
[3] S. Fleischer, I. Sh. Averbukh, Y. Prior, *Phys. Rev. A* **2006**, *74*, 041403.
[4] S. Fleischer, I. Sh. Averbukh, Y. Prior, *Phys. Rev. Lett.* **2007**, *99*, 093002.
[5] S. Fleischer, I. Sh. Averbukh, Y. Prior, *J. Phys. B* **2008**, *41*, 074018.
[6] S. Fleischer, Y. Khodorkovsky, I. Sh. Averbukh, Y. Prior, *New J. Phys.* **2009**, *11*, 105039.
[7] Y. Khodorkovsky, H. Hasegawa, Y. Ohshima, I. Sh. Averbukh, *Phys. Rev. A* **2011**, *83*, 023423.
[8] E. Gershnabel, I. Sh. Averbukh, *Phys. Rev. Lett.* **2010**, *104*, 153001.
[9] E. Gershnabel, I. Sh. Averbukh, *J. Chem. Phys.* **2011**, *134*, 054304.
[10] Y. Khodorkovsky, I. Sh. Averbukh, E. Pollak, *J. Phys. Condens. Matter* **2010**, *22*, 304004.
[11] M. A. Duguay, J. W. Hansen, *Appl. Phys. Lett.* **1969**, *15*, 6.
[12] D. Normand, L. A. Lompre, C. Cornaggia, *J. Phys. B* **1992**, *25*, L497.
[13] P. Dietrich, D. T. Strickland, M. Laberge, P. B. Corkum, *Phys. Rev. A* **1993**, *47*, 2305.
[14] G. R. Kumar, P. Gross, C. P. Safvan, F. A. Rajgara, D. Mathur, *Phys. Rev. A* **1996**, *53*, 3098.
[15] B. A. Zon, B. G. Katsnelson, *Sov. Phys. JETP* **1976**, *42*, 595.
[16] B. Friedrich, D. Herschbach, *Phys. Rev. Lett.* **1995**, *74*, 4623; B. Friedrich, D. Herschbach, *J. Phys. Chem.* **1995**, *99*, 15686.
[17] W. Kim, P. M. Felker, *J. Chem. Phys.* **1996**, *104*, 1147.
[18] C. H. Lin, J. P. Heritage, T. K. Gustafson, *Appl. Phys. Lett.* **1971**, *19*, 397; J. P. Heritage, T. K. Gustafson, C. H. Lin, *Phys. Rev. Lett.* **1975**, *34*, 1299.
[19] P. M. Felker, *J. Phys. Chem.* **1992**, *96*, 7844.
[20] T. Seideman, *J. Chem. Phys.* **1995**, *103*, 7887; T. Seideman, *J. Chem. Phys.* **1997**, *106*, 2881.
[21] J. Ortigoso, M. Rodríguez, M. Gupta, B. Friedrich, *J. Chem. Phys.* **1999**, *110*, 3870.
[22] L. Cai, J. Marango, B. Friedrich, *Phys. Rev. Lett.* **2001**, *86*, 775.
[23] T. Seideman, *Phys. Rev. Lett.* **1999**, *83*, 4971.
[24] M. Machholm, N. E. Henriksen, *Phys. Rev. Lett.* **2001**, *87*, 193001.
[25] M. Machholm, *J. Chem. Phys.* **2001**, *115*, 10724.
[26] C. M. Dion, A. Keller, O. Atabek, *Eur. Phys. J. D* **2001**, *14*, 249.
[27] F. Rosca-Pruna, M. J. J. Vrakking, *Phys. Rev. Lett.* **2001**, *87*, 153902.
[28] I. Sh. Averbukh, R. Arvieu, *Phys. Rev. Lett.* **2001**, *87*, 163601.
[29] I. Sh. Averbukh, R. Arvieu, M. Leibscher, **2002**, quant-ph/0202051.
[30] E. Peronne, M. D. Poulsen, C. Z. Bisgaard, H. Stapelfeldt, T. Seideman, *Phys. Rev. Lett.* **2003**, *91*, 043003.
[31] I. Sh. Averbukh, N. F. Perelman, *Phys. Lett. A* **1989**, *139*, 449.
[32] C. Leichtle, I. Sh. Averbukh, W. P. Schleich, *Phys. Rev. Lett.* **1996**, *77*, 3999.
[33] C. Leichtle, I. Sh. Averbukh, W. P. Schleich, *Phys. Rev. A* **1996**, *54*, 5299–5312.
[34] H. Stapelfeldt, T. Seideman, *Rev. Mod. Phys.* **2003**, *75*, 543.
[35] E. A. Shapiro, M. Spanner, M. Y. Ivanov, *Phys. Rev. Lett.* **2003**, *91*, 237901.
[36] E. A. Shapiro, I. Khavkine, M. Spanner, M. Y. Ivanov, *Phys. Rev. A* **2003**, *67*, 013406.
[37] K. F. Lee, D. M. Villeneuve, P. B. Corkum, E. A. Shapiro, *Phys. Rev. Lett.* **2004**, *93*, 233601.
[38] A. V. Sokolov, *Opt. Lett.* **1999**, *24*, 1248.
[39] R. A. Bartels, T. C. Weinacht, N. Wagner, M. Baertschy, C. H. Greene, M. M. Murnane, H. C. Kapteyn, *Phys. Rev. Lett.* **2002**, *88*, 013903.
[40] M. Comstock, V. V. Lozovoy, M. Dantus, *Chem. Phys. Lett.* **2003**, *372*, 739.
[41] D. Shafir, Y. Mairesse, D. M. Villeneuve, P. B. Corkum, N. Dudovich, *Nat. Phys.* **2009**, *5*, 412.
[42] B. K. McFarland, J. P. Farrell, P. H. Bucksbaum, M. Gühr, *Science* **2008**, *322*, 1232.
[43] L. Holmegaard, J. L. Hansen, L. Kalhøj, S. L. Kragh, H. Stapelfeldt, F. Filsinger, J. Küpper, G. Meijer, D. Dimitrovski, M. Abu-samha, C. P. J. Martiny, L. B. Madsen, *Nat. Phys.* **2010**, *6*, 428–432.
[44] H. Sakai, C. P. Safvan, J. J. Larsen, K. M. Hilligsøe, K. Hald, H. Stapelfeldt, *J. Chem. Phys.* **1999**, *110*, 10235.
[45] L. Bergé, S. Skupin, F. Lederer, G. Méjean, J. Yu, J. Kasparian, E. Salmon, J. P. Wolf, M. Rodriguez, L. Wöste, R. Bourayou, R. Sauerbrey, *Phys. Rev. Lett.* **2004**, *92*, 22.
[46] Z. Jin, J. Zhang, M. H. Xu, X. Lu, Y. T. Li, Z. H. Wang, Z. Y. Wei, *Opt. Express* **2005**, *13*, 10424 .
[47] F. Calegari, C. Vozzi, E. Benedetti, S. Gasilov, G. Sansone, M. Nisoli, S. De Silvestri, S. Stagira in *Conference on Lasers and Electro-Optics/Quantum Electronics and Laser Science Conference and Photonic Applications Systems Technologies 2008 Technical Digest*, Optical Society of America, Washington, DC, **2008**, QTuF3.
[48] J. Hajdu, *Current Opinion in Structural Biology* **2000**, *10*, 569–573.
[49] R. Neutze, R. Wouts, D. van der Spoel, E. Weckert, J. Hajdu, *Nature* **2000**, *406*, 752–757.
[50] M. Leibscher, I. Sh. Averbukh, H. Rabitz, *Phys. Rev. Lett.* **2003**, *90*, 213001.
[51] I. Sh. Averbukh, R. Arvieu, M. Leibscher in *Coherence and Quantum Optics VIII* (Eds.: N. P. Bigelow, J. H. Eberly, C. R. Stroud, Jr., I. A. Walmsley), Kluwer, NY, **2003**, pp. 71–86.
[52] M. Leibscher, I. Sh. Averbukh, *Phys. Rev. A* **2002**, *65*, 053816.

[53] M. Leibscher, I. Sh. Averbukh, H. Rabitz, *Phys. Rev. A* **2004**, *69*, 013402.
[54] K. F. Lee, I. V. Litvinyuk, P. W. Dooley, M. Spanner, D. M. Villeneuve, P. B. Corkum, *J. Phys. B* **2004**, *37*, L43.
[55] D. Pinkham, K. E. Mooney, R. R. Jones, *Phys Rev. A* **2007**, *75*, 013422.
[56] J. P. Cryan, P. H. Bucksbaum, R. N. Coffee, *Phys. Rev. A* **2009**, *80*, 063412.
[57] V. Renard, M. Renard, S. Guérin, Y. T. Pashayan, B. Lavorel, O. Faucher, H. R. Jauslin, *Phys. Rev. Lett.* **2003**, *90*, 153601.
[58] H. Sakai, C. P. Safvan, J. J. Larsen, K. M. Hilligsøe, K. Hald, H. Stapelfeldt, *J. Chem. Phys.* **1999**, *110*, 10235.
[59] D. Normand, L. A. Lompre, C. Cornaggia, *J. Phys. B* **1992**, *25*, L497.
[60] J. Karczmarek, J. Wright, P. Corkum, M. Ivanov, *Phys. Rev. Lett.* **1999**, *82*, 3420.
[61] Y. Prior, *Appl. Opt.* **1980**, *19*, 1741.
[62] E. J. Brown, Q. Zhang, M. Dantus, *J. Chem. Phys.* **1999**, *110*, 12.
[63] E. J. Brown, I. Pastirk, M. Dantus, *J. Phys. Chem. A* **2001**, *105*, 8004–8010.
[64] J. J. Larsen, H. Sakai, C. P. Safven, I. Wendt-Larsen, H. Stapelfeldt, *J. Chem. Phys.* **1999**, *111*, 17.
[65] D. Zeidler, A. B. Bardon, A. Staudte, D. M. Villeneuve, R. Doerner, P. B. Corkum, *J. Phys. B* **2006**, *39*, L159–L166.
[66] J. J. Larsen, I. Wendt-Larsed, H. Stapelfeldt, *Phys. Rev. Lett.* **1999**, *83*, 1123.
[67] D. Pinkham, R. R. Jones, *Phys. Rev. A* **2005**, *72*, 023418.
[68] M. Renard, E. Hertz, B. Lavorel, O. Faucher, *Phys. Rev. A* **2004**, *69*, 043401.
[69] M. Spanner, E. A. Shapiro, M. Ivanov, *Phys. Rev. Lett.* **2004**, *92*, 9.
[70] R. Bocchieri, A. Loinger, *Phys. Rev.* **1957**, *107*, 337.
[71] James E. Bayfield, *Quantum Evolution: An Introduction to Time-Dependent Quantum Mechanics*, Wiley, New York, **1999**.
[72] M. Leibscher, I. Sh. Averbukh, P. Rozmej, R. Arvieu, *Phys Rev. A* **2004**, *69*, 032102.
[73] G. B. Arfken, H. J. Weber, *Mathematical Methods for Physicists*, 6th ed., Academic Press, San Diego, **2005**.
[74] S. Fleischer, Y. Zhou, R. W. Field, K. A. Nelson, *Phys. Rev. Lett.* **2011**, *107*, 163603.
[75] P. R. Bunker, P. Jensen, *Molecular Symmetry and Spectroscopy*, 2nd ed., NRC Research Press, Ottawa, **1998**.
[76] N. Gedik, J. Orenstein, *Opt. Lett.* **2004**, *29*, 2109.
[77] M. Renard, E. Hertz, S. Guérin, H. R. Jauslin, B. Lavorel, O. Faucher, *Phys. Rev. A* **2005**, *72*, 025401.
[78] K. F. Lee, E. A. Shapiro, D. M. Villeneuve, P. B. Corkum, *Phys. Rev. A* **2006**, *73*, 033403.
[79] L. Yuan, S. W. Teitelbaum, A. Robinson, A. S. Mullin, *Proc. Natl. Acad. Sci. USA* **2011**, *108*, 6877.
[80] K. Kitano, H. Hasegawa, Y. Ohshima, *Phys. Rev. Lett.* **2009**, *103*, 223002.
[81] H. Hasegawa, Y. Ohshima, *Chem. Phys. Lett.* **2008**, *454*, 148.
[82] R. M. Logan, R. E. Stickney, *J. Chem. Phys.* **1966**, *44*, 195.
[83] J. D. Doll, *J. Chem. Phys.* **1973**, *59*, 1038.
[84] Y. Khodorkovsky, J. R. Manson, I. Sh. Averbukh, arXiv:1107. 0818v1 [physics. chem-ph], **2011**.
[85] H. Stapelfeldt, H. Sakai, E. Constant, P. B. Corkum, *Phys. Rev. Lett.* **1997**, *79*, 2787; H. Sakai, A. Tarasevitch, J. Danilov, H. Stapelfeldt, R. W. Yip, C. Ellert, E. Constant, P. B. Corkum, *Phys. Rev. A* **1998**, *57*, 2794.
[86] S. M. Purcell, P. F. Barker, *Phys. Rev. Lett.* **2009**, *103*, 153001.
[87] E. Gershnabel, I. Sh. Averbukh, R. J. Gordon, *Phys. Rev. A* **2006**, *74*, 053414.
[88] E. Gershnabel, I. Sh. Averbukh, *Phys. Rev. A* **2010**, *82*, 033401.
[89] H. Goldstein, C. Poole, J. Safko, *Classical Mechanics*, 3rd ed., Addison Wesley, USA, **2001**.
[90] L. D. Landau, E. M. Lifshitz, *Mechanics*, 3rd ed., Butterworth-Heinemann, UK, **1976**.
[91] P. Dugourd, I. Compagnon, F. Lepine, R. Antoine, D. Rayane, M. Broyer, *Chem. Phys. Lett.* **2001**, *336*, 511.
[92] D. M. Villeneuve, S. A. Aseyev, P. Dietrich, M. Spanner, M. Yu. Ivanov, P. B. Corkum, *Phys. Rev. Lett.* **2000**, *85*, 542.
[93] M. Spanner, M. Yu. Ivanov, *J. Chem. Phys.* **2001**, *114*, 3456; M. Spanner, K. M. Davitt, M. Yu. Ivanov, *J. Chem. Phys.* **2001**, *115*, 8403.
[94] A. G. York, *Opt. Express* **2009**, *17*, 13671.
[95] M. Lapert, E. Hertz, S. Guérin, D. Sugny, *Phys. Rev. A* **2009**, *80*, R051403.
[96] B. S. Zhao, H. S. Chung, K. Cho, S. H. Lee, S. Hwang, J. Yu, Y. H. Ahn, J. Y. Sohn, D. S. Kim, W. K. Kang, D. S. Chung, *Phys. Rev. Lett.* **2000**, *85*, 2705; H. S. Chung, B. S. Zhao, S. H. Lee, S. Hwang, K. Cho, S. H. Shim, S. M. Lim, W. K. Kang, D. S. Chung, *J. Chem. Phys.* **2001**, *114*, 8293.
[97] B. S. Zhao, S. H. Lee, H. S. Chung, S. Hwang, W. K. Kang, B. Friedrich, D. S. Chung, *J. Chem. Phys.* **2003**, *119*, 8905.
[98] R. Glauber, F. Haake, *Phys. Rev. A* **1976**, *13*, 357.
[99] F. Arecchi, E. Courtens, R. Gilmore, H. Thomas, *Phys. Rev. A* **1972**, *6*, 2211.
[100] D. A. Baugh, D. Y. Kim, V. A. Cho, L. C. Pipes, J. C. Petteway, C. D. Fuglesang, *Chem. Phys. Lett.* **1994**, *219*, 207.
[101] L. Holmegaard, J. H. Nielsen, I. Nevo, H. Stapelfeldt, F. Filsinger, J. Küpper, G. Meijer, *Phys. Rev. Lett.* **2009**, *102*, 023001; F. Filsinger, J. Küpper, G. Meijer, L. Holmegaard, J. H. Nielsen, I. Nevo, J. L. Hansen, H. Stapelfeldt, *J. Chem. Phys.* **2009**, *131*, 064309.
[102] C. Cohen-Tannoudji, B. Diu, F. Laloe, *Quantum Mechanics*, Wiley-Interscience, Hoboken, **2006**.
[103] E. O. Steinborn, K. Ruedenberg in *Advances in Quantum Chemistry, Vol. 7* (Ed.: P.-O. Löwdin), Academic Press, NY, **1973**, p. 1–81.
[104] J. Floß, E. Gershnabel, I. Sh. Averbukh, *Phys. Rev. A* **2011**, *83*, 025401.
[105] E. Gershnabel, M. Shapiro, I. Sh. Averbukh, *J. Chem. Phys.* **2011**, *135*, 194310.
[106] E. Gershnabel, I. Sh. Averbukh, *J. Chem. Phys.* **2011**, *135*, 084307.

Received: November 24, 2011
Accepted: December 26, 2011
Published online: April 27, 2012

